California Margin temperatures modulate regional circulation and extreme summer precipitation in the desert Southwest

Tripti Bhattacharya,[1*] Ran Feng,[2] Chris R. Maupin,[3] Sloan Coats [4]
Peter R. Brennan,[1], Elizabeth Carter[5]

[1]Department of Earth and Environmental Sciences, Syracuse University, Syracuse NY USA
[2]Department of Geosciences, University of Connecticut, Storrs CT
[3]Department of Geography, Texas A&M University, College Station, TX, USA
[4]Department of Earth Sciences, University of Hawai'i at Manoa, Honolulu, HI, USA
[5]Civil and Environmental Engineering, Syracuse University, Syracuse, NY USA

*To whom correspondence should be addressed; E-mail: trbhatta@syr.edu.

This paper is a post-print has been published in Environmental Research Letters, doi:
10.1088/1748-9326/acfd43.

California Margin temperatures modulate regional circulation and extreme summer precipitation in the desert Southwest

Tripti Bhattacharya[1*], Ran Feng[2], Christopher R. Maupin[3], Sloan Coats[4], Peter R. Brennan[1], Elizabeth Carter[5]

[1*]Department of Earth and Environmental Sciences, Syracuse University, Syracuse NY USA
[2]Department of Earth Sciences, University of Connecticut, Storrs, CT, USA
[3]Department of Geography, Texas A&M University, College Station, TX, USA
[4]Department of Earth Sciences, University of Hawai'i at Manoa, Honolulu, HI, USA
[5]Civil and Environmental Engineering, Syracuse University, Syracuse, NY USA
* Corresponding Author

E-mail: `trbhatta@syr.edu`

April 2023

Abstract. In August 2022, Death Valley, the driest place in North America, experienced record flooding from summertime rainfall associated with the North American Monsoon (NAM). Given the socioeconomic cost of these type of events, there is a dire need to understand their drivers and future statistics. Existing theory predicts that increases in the intensity of precipitation is a robust response to anthropogenic warming. Paleoclimatic evidence suggests that northeast Pacific sea surface temperature (SST) variability could further intensify summertime NAM rainfall over the desert southwest. Drawing on this paleoclimatic evidence, we use historical observations and reanalyses to test the hypothesis that warm SSTs on the southern California margin are linked to more frequent extreme precipitation events in the NAM domain. We find that summers with above-average coastal SSTs are more favorable to moist convection in the northern edge of the NAM domain (southern California, Arizona, New Mexico, and the southern Great Basin). This is because warmer SSTs drive circulation changes that increase moisture flux into the desert southwest, driving more frequent precipitation extremes and increases in seasonal rainfall totals. These results, which are robust across observational products, establish a linkage between marine and terrestrial extremes, since summers with anomalously warm SSTs on the California margin have been linked to seasonal or multi-year northeast Pacific marine heatwaves. However, current generation earth system models (ESMs) struggle to reproduce the observed relationship between coastal SSTs and NAM precipitation. Across models, there is a strong negative relationship between the magnitude of an ESM's warm SST bias on the California margin and its skill at reproducing the correlation with desert southwest rainfall. Given persistent northeast Pacific SST biases in ESMs, our results suggest that efforts to improve representation of climatological SSTs are crucial for accurately predicting future changes in hydroclimate extremes in the desert southwest.

Keywords: North American Monsoon, extreme rainfall, southwest hydroclimate

1. Introduction

In August 2022, regions of the desert southwest including Death Valley, the driest place in North America, experienced once-in-a thousand year flooding. This was a result of summertime storms that dumped up to 75% of normal annual precipitation amounts in the span of a few hours (Canon, 2022). These storms occurred at the northern side of the North American Monsoon (NAM), the primary source of summer rainfall in southwestern North America (Cook and Seager, 2013; Adams and Comrie, 1997). These types of events are associated with loss of life and infrastructure damage. In addition, above-average monsoon rainfall has been linked to increases in invasive plant biomass, increasing fire risk (Moloney et al., 2019). The profound socioeconomic and ecological impacts of the region's precipitation extremes highlight the need to understand the mechanisms underlying their variability.

An increase in precipitation intensity is expected as a result of global warming, since saturation specific humidity increases with temperature (O'Gorman, 2015). In the NAM domain, earth system models (ESMs) and regional models all suggest that warming tends to intensify individual storms, despite predictions of an overall decrease in summer rainfall by the end of the 21st century (albeit with considerable structural uncertainty–(Pascale et al., 2017, 2018; Almazroui et al., 2021; Moon and Ha, 2020; Meyer and Jin, 2017)). Nevertheless, the entire summer of 2022 featured above-average rainfall, especially on the northern edge of the NAM domain (Figure S1,a). Not only were rainfall rates above average in Nevada, Arizona, and New Mexico, but values of daily outgoing longwave radiation (OLR) show a systematic shift to a longer left tail, suggesting a greater frequency of cooler cloud tops associated with convective rainfall.

We hypothesize that north Pacific SST variability helped drive these higher rainfall rates. The summer of 2022 featured positive SST anomalies in coastal regions of the northeast Pacific (NEP), as well as a La Niña event in the eastern equatorial Pacific (EEP). Observational analyses have shown that La Niña events feature a stronger monsoon ridge, enhancing the strength of the circulation (Castro et al., 2001). Previous analyses of intraseasonal variability in the monsoon found that cool conditions in the EEP cold tongue could drive an earlier monsoon onset (Castro et al., 2001; Bieda et al., 2009). Modeling results, however, are equivocal about the impact of extratropical Pacific SST anomalies on the monsoon. Some studies suggest that warm NEP SST anomalies, similar to the configuration observed in summer 2022, should weaken the monsoon (Castro et al., 2001). In contrast, more recent work suggests that these types of events should strengthen the monsoon (Fu et al., 2022; Beaudin et al., 2023). The latter two studies used idealized atmosphere-only simulations forced by fixed SSTs, and require corroboration by observations. Yet, observations and paleoclimatic reconstructions are equivocal about the relationship between southwest summer precipitation and large-scale SST patterns (Carrillo et al., 2016; Demaria et al., 2019; Griffin et al., 2013; Coats et al., 2015). Given these contradictory findings, more work is needed to contextualize the role of SST variability in driving extremes similar to summer 2022. Along these lines, paleoclimatic evidence from past warm intervals has identified a link between warm SSTs off the southern California margin and an intensification of monsoon rainfall (Bhattacharya et al., 2022; Fu et al., 2022). If this relationship holds in the modern, it suggests that warm NEP SSTs, especially on the California Margin, would have played a role in August 2022 flooding.

In this study, we explore the link between SST on the CA margin and precipitation in the northern NAM domain. Because of our interest in events similar to the Death Valley flooding in August 2022, we focus on the northern edge of the NAM domain, or regions of the desert southwest in Arizona, New Mexico, California and Nevada. Using observational data, reanalyses, and ESM simulations, we analyze the relationship between large-scale SST patterns and both extreme precipitation and seasonal precipitation totals. We show that summers of a greater frequency of days with extreme precipitation in the northern NAM domain tend to co-occur with intervals of warm SSTs on the CA margin. There is also a statistically significant relationship between CA margin SSTs and seasonally-averaged summertime rainfall in the northern NAM domain. Our results therefore provide important context for the processes underlying recent extreme precipitation in the desert southwest, and also identify a mechanism of inter-annual variability in extremes that may continue to influence regional precipitation into the 21st century. However, the ability of Coupled Model Intercomparison Project (CMIP) phase 5 and 6 ESMs to reproduce this relationship is highly variable, and depends in part on the magnitude of a model's warm SST bias on the CA margin. This has implications for our ability to use ESMs to estimate future changes in extreme precipitation, signal-to-noise ratios, and hydroclimate-related risks in the desert southwest.

2. Data and Methods

2.1. Composite Analyses and Conditional Probability

Our work focuses on the northern NAM domain, consisting of land regions of the desert southwest between 28 to 37 °N and 115 to 108 °W. We used daily Global Precipitation Climatology Centre's (GPCC) 1.0°data to define the 95th percentile of daily precipitation rates at each grid point. This threshold, otherwise known as 'p95', is a widely accepted metric of extreme precipitation (Sillmann et al., 2013). We then calculated the number of days between June 14th and the end of September in each year that exceed p95 for the interval between 1982 and 2014 (Schneider et al., 2008). While heavy rainfall is relatively rare in this desert setting, events like August 2022 highlight the profound impact of extremes.

To contextualize extreme precipitation, we analyzed composites of daily fields of outgoing longwave radiation (OLR), as an indicator of cold cloud tops and convective rainfall, from NOAA (Liebmann and Smith, 1996); zonal and meridional moisture flux; and daily maximum 3-hourly convectively available potential energy (CAPE, a measure of energetic favorability of the atmosphere for deep convection and rainfall) from the North American Regional Reanalysis (NARR–(Mesinger et al., 2006)). We also analyze monthly sea level pressure and 850 mb geopotential heights from the NCEP-NCAR reanalysis (Kalnay et al., 1996). In order to link changes in the frequency of daily precipitation extremes to SST, we analyzed anomalies of monthly SST (Ishii et al., 2005) associated with summers that contain the greatest frequency of extreme precipitation.

We also quantified the probability of seeing a summer with above-average days (e.g., greater than 6 days) of extreme precipitation in the northern NAM domain in years with anomalously warm CA margin temperatures (years where SST anomalies 25 and 32 °N and 125 and 110 °W are $> 1\sigma$ above average). This is the conditional probability that a summer will have greater than 6 days of precipitation exceeding p95 given anomalously warm SSTs on the CA margin. We assessed this probability for warm CA margin SST anomalies at different lead times (e.g., the preceding April-June SSTs), to see whether preceding CA margin SSTs can serve as predictors of northern NAM domain precipitation extremes. The statistical significance of these conditional probabilities was calculated using a 1-sided binomial test to assess whether it was significantly different from random chance (i.e., that the observed conditional probability is not significantly larger than expected from a process with a 50% probability of occurrence (Wilks, 2011)).

2.2. Correlation Analysis and Comparison with ESM Simulations

We quantified the relationship between CA margin SSTs and monthly mean precipitation over the northern NAM domain by correlating the same index of CA margin SSTs anomalies with monthly mean precipitation from multiple precipitation products to establish the robustness of the relationship (0.25 °GPCC product between 1960 and 2020, the CPC merged analysis of precipitation (CPC), the Global Precipitation Climatology Project (GPCP), and the NARR (Schneider et al., 2008; Xie et al., 2007; Adler et al., 2018; Mesinger et al., 2006)). We also analyze the correlation of our SST index and fields of sea level pressure (SLP), 850 mb geopotential height (Kalnay et al., 1996) between 1950 and 2020, and zonal and meridional moisture flux between 1979 and 2022 (NARR, (Mesinger et al., 2006)). The focus on monthly mean correlations facilitates comparison to CMIP models, since only monthly mean fields are available for many models.

To determine the extent to which CMIP5 and CMIP6 ESMs reproduce the observed relationship between CA margin SSTs, precipitation, and circulation, we analyzed historical model simulations from 23 ESMs, including several from the HighResMIP project (Chang et al., 2020; Haarsma et al., 2016; Eyring et al., 2016) (Table S1). Because the set of simulations we analyze differ in their input forcing datasets (e.g., CMIP5 vs. CMIP6 historical simulations), we focused on analyzing the sensitivity of precipitation to CA margin SSTs instead of making inferences about how trends in CA margin SSTs may influence the future behavior of the NAM. We quantified the linear correlation between southern CA Margin SSTs (e.g., the previously defined SST index, averaged between 25 and 32 °N and 125 and 110 °W) and northern NAM domain precipitation (e.g., the area between 28 to 37 °N and 115 to 108 °W). Finally, we compared the correlation between the SST index and large-scale fields (e.g. vertically integrated moisture flux, 850 mb geopotential height, and SLP) between a subset of models that perform well (e.g. exhibit a realistic SST-precipitation correlation) and a subset of models that perform poorly. This analysis required regridding historical output to a common 1°by 1°grid before computing cross-correlations between each models' SST index and large-scale fields (see SI).

3. Results and Discussion

3.1. California Margin temperatures and northern NAM domain precipitation

Between 1979 and 2014, 5 summers featured the greatest number of days with rainfall exceeding p95 (Sillmann et al., 2013; Cavazos et al., 2008) (Figure 1a). These years also show a statistically significant shift to larger values of daily maximum 3-hourly CAPE, indicating an increase in the energetic potential of the atmosphere to generate deep convection (Figure 1d). This shift in CAPE is accompanied by a shift in daily OLR indicative of colder cloud tops associated with deep convection (Figure S2). These shifts in the distribution of CAPE and OLR suggest that summers with greater extreme precipitation days featured an atmospheric environment that was more conducive to convective activity. This is consistent with station-based observations associated with the initiation of August 9th-10th storms over Las Vegas (Figure S11). Atmospheric soundings from Las Vegas indicate a shift to low-level southerly flow overnight, coincident with the development of a deep, moist layer and stronger instability despite relatively low early morning surface temperatures. This results in a near-doubling of CAPE(Figure S11).

The composite SST pattern associated with these five summers reveals a 'horseshoe' pattern of warmth in the NEP similar to the warm phase of Pacific decadal variability and the extratropical expression of warm ENSO events (Di Lorenzo et al., 2023) (Figure 1d), with stronger anomalies near Alaska and off the CA margin. The extratropical portion of this SST pattern resembles the SST anomaly pattern from summer 2022 (Figure S1d). However, unlike 2022, the EEP cold tongue shows only weakly positive SST anomalies, reflecting that these 5 years featured different phases of ENSO. While some years featured La Niña events (e.g., 1984, 1990, 1996), others had moderate or decaying El Niño events (e.g., 1983, 2014). The lack of a consistent ENSO phase reflects the relatively weak relationship between ENSO and NAM precipitation (Castro et al., 2001). It also suggests that NEP SST patterns, especially on the CA margin, may play a more important role in modulating the NAM than the EEP, although we note that tropical and extratropical variability are connected (Di Lorenzo et al., 2023). It is notable that at least two of the five years used in this analysis coincide with significant seasonally-persistent extratropical marine heat waves (e.g., 1990, 2014) (Capotondi et al., 2022), suggesting a link between marine and atmospheric extremes.

3.2. Implications for Seasonal Prediction

The association between CA margin SSTs and northern NAM precipitation extremes raises the possibility that coastal SSTs could aid in efforts to predict inter-seasonal precipitation extremes. This may especially be true given the strong seasonal persistence of temperature anomalies in this region on seasonal timescales, despite some sub-seasonal variability (Wei et al., 2021) (Figure S3). To test this possibility, we quantified the conditional probability of a summer containing an above-average number of days exceeding p95 given anomalously warm CA margin temperatures (e.g., greater than 1σ above average). When CA margin SSTs are 1σ above average in JAS, there is a 85% probability of seeing greater than average days with precipitation exceeding p95 (Figure 2). Warm CA margin SST anomalies during early summer (JJA, MJJ) and spring (AMJ) are also associated with summers with above-average extreme precipitation days. Each of these relationships are statistically significant at the 95% level (1-sided binomial test (Wilks, 2011)). These results highlight the potential utility of coastal SSTs for predicting summers with greater extreme precipitation days in the desert southwest.

3.3. Mechanism of SST-Monsoon Linkage

Consistent with an energetic environment more conducive to summertime convection, the summers highlighted in Figure 1a are associated with higher monthly mean rainfall rates over the northern NAM domain. They are also associated with higher geopotential heights over the North American continent and the southern CA margin, with a trough to the northwest (Figure 1e, S11, S14). This is coupled with stronger southwesterly moisture flux, and a cyclonic circulation anomaly centered over Baja California, similar to the changes observated during the August 2022 floods (Figure 1g, S11). The anomalous moisture flux results in a large increase in precipitable water over Baja California, the northern NAM domain, and California margin, with an almost 50% increase in humidity in some of these regions (Figure 1g,S4). Changes in evaporation are modest compared to changes in moisture flux and precipitable water (Figure 1h). The link between total precipitable water off the southern California coast and extreme NAM precipitation has been noted in studies of individual flood events (Yang et al., 2017; Mazon et al., 2016), but the link to coastal SSTs and large-scale circulation has not been explicitly studied.

Correlations of NARR precipitation with the CA margin SST index are largely positive, especially over Baja California and the southern Great Basin, northern margin of the present-day NAM domain (Figure 2a). This correlation pattern is statistically significant and robust across multiple observational products (Figure S6,S7). CA margin SSTs are correlated with stronger southerly moisture flux over Baja and coastal California (Figure 2b), consistent with composites showing southwesterly moisture transport during extreme precipitation summers (Figure 1g). Over the Gulf of California, this correlation represents an enhancement of the climatological southerly moisture transport (Bordoni and Stevens, 2006; Johnson and Delworth, 2023). Over the California margin, positive correlations with meridional moisture transport reflect a weakening of northerly and easterly flow that diverges moisture away from coastal southern California (Figure 2b).

We contend that warm CA margin SST anomalies drive stronger southwesterly moisture transport because they help weaken the southeast edge of the North Pacific subtropical high pressure system (NPSH). Correlations with 850 mb geopotential heights reveal that warm CA margin SSTs are associated with a weakening of the geopotential gradient on the southern edge of the NPSH (Figure 2c)). Further support for this comes from the strong negative correlation between CA margin SSTs and SLP on the southeast edge of the NPSH (Figure 2d). Given previous work showing that cool SSTs over eastern ocean margins help maintain the strength of the subtropical highs, we suggest that anomalously warm temperatures on the CA margin weaken the NPSH in this region by reducing local static stability (Seager et al., 2003; Bhattacharya, 2022). The strong negative correlation between CA margin SSTs and SLP centered west of Baja California and extending along the edge of the NPSH is not present in the correlation field between ENSO and SLP (Figure S8). This is likely because variability in CA margin SSTs reflects additional processes beyond ENSO-induced variability (Di Lorenzo et al., 2023). There is some similarity between the SLP correlation pattern with CA margin SSTs and the PDO, consistent with recent findings that the PDO modulates SST variability and MHW intensity off Baja California (Figure S8)(Ren et al., 2023).

Our analyses suggest that CA margin SSTs weaken the southeast edge of the NPSH, favoring stronger moisture flux into the desert southwest. Subsequent increases in humidity would promote higher dewpoints and fuel instability over these normally dry desert regions. From this perspective, warm CA margin SSTs help enhance the positive CAPE generated by a warm summertime Gulf of California (Johnson and Delworth, 2023). Given that NPSH strength and underlying SSTs are tightly coupled via air-sea interactions (Seager et al., 2003), observations alone are insufficient to establish the direction of causality between SST and NPSH strength. In fact, outflow from the NAM may help amplify SST anomalies on the California margin (Clemesha et al., 2023). However, our results agree with several atmosphere-only regional and global simulations showing that CA margin SSTs play a causal role in driving a cyclonic circulation anomaly and stronger meridional moisture flux into the southwest (Beaudin et al., 2023; Fu et al., 2022).

3.4. Model Representation of SST-Summer Rainfall Relationship

Figures 1 and 2 suggest that summers with warm CA margin SSTs not only feature more extreme precipitation days, but also see an atmospheric shift conducive to higher seasonal rainfall totals. Accurately representing this SST-monsoon linkage is therefore key for quantifying and predicting future risks related to extreme precipitation (e.g., flooding, infrastructure damage). Since most future projections of the NAM system rely on downscaled (or direct) output from ESMs, we next assess whether ESMs reproduce the CA margin SST - monsoon relationship found in observational products (Figure 2).

Only a small subset of ESMs simulate a similar correlation between CA margin SST and northern NAM domain precipitation as compared to observational products. Furthermore, there is a significant negative correlation between a given models' warm SST bias on the CA margin and the strength of the correlation with northern NAM domain precipitation: ESMs that are too warm in the CA margin relative to observations underestimate the correlation between summer precipitation and CA margin SSTs (Figure 3). For two ESMs, increasing resolution improves both the SST bias and the strength of the correlation (Figure 3). This coheres with previous findings that higher resolution ESMs perform better at simulating the NAM because of their ability to resolve topography and produce realistic statistics of transient disturbances (Pascale et al., 2016; Meyer and Jin, 2017; Varuolo-Clarke et al., 2019). However, higher resolution does not always improve the correlation: the higher resolution configuration of the CNRM model produces a weaker CA Margin SST-NAM summer precipitation correlation than its low resolution counterpart (Figure 3). In addition, higher resolution models do not necessarily have a more realistic climatology of NAM precipitation (Figure S9). Instead, we suggest that biases in their simulation of the large-scale climate play an important role in models' ability to capture coupling between SST variability, atmospheric circulation, and regional hydroclimate, as captured in Figure 3.

To further investigate this hypothesis, we quantify the correlation between SLP, 850 mb geopotential heights, and meridional moisture flux for the ESMs that are best able to (CESM1.3-HR; CanESM5-1; ACCESS-CM2; MPI-ESM1-2-HR) and least able to (MIROC6; FIO-ESM2; NESM3) reproduce the observed SST-monsoon linkage (Figure 4a). Model precipitation correlations are shown in Figure S10. SLP fields reveal that the best performing models produce a NPSH that is extended slightly farther southeast and weaker than the worst performing models (e.g., 1012 mb contour that extends south of 20°N, similar to observations (Figure 2c)).

The best performing models produce a strong negative correlation between SLP and the CA margin SST index, especially on the southeast edge of the NPSH (Figure 4a). This resembles the pattern seen in observational data (Figure 4b). In contrast, the worst performing models produce the wrong sign of correlation between the CA margin SST index and SLP. The best performing models also produce positive correlations between CA margin SSTs and 850-mb geopotential heights over the California Margin and a negative correlation to the west, similar albeit slightly different in pattern to observations (Figure 4b,Figure 2a). The worst performing models only produce a localized region of positive correlation, failing to reproduce the east-west dipole in correlation seen in observations. These differences in large-scale correlation patterns directly translate into differences in the correlation pattern across models between CA margin SSTs and moisture flux: the best performing models produce a much stronger correlation between meridional moisture transport and the CA margin SST index than the worst performing models (Figure 4c,f), especially in the regions over Baja California and southern California.

These results suggest that the difference in skill between the best and worst performing models in our analysis relates to the fact that the best performing models exhibit a tighter coupling (and stronger correlation) between the underlying anomalies of SST, atmospheric circulation (e.g., the NPSH), and moisture flux than seen in the worst performing models. This appears to be a direct function of the stronger warm SST bias on the California margin in the worst performing models. We hypothesize that for models with a strong warm bias on the CA margin, a given SST anomaly represents a smaller fractional or percent change in SST and hence a smaller perturbation to the overlying atmosphere. Therefore, in more strongly warm biased models, a given SST anomaly may be less efficient at altering atmospheric circulation (e.g., weakening static stability). ESMs with a stronger warm bias may therefore generate less variability in the southeast edge of the NPSH, as well as a weaker correlation between SST, moisture flux, and NAM precipitation.

4. Conclusions

In this paper, we used observational data and reanalyses to demonstrate a linkage between California Margin SSTs and precipitation over the US southwest, Baja California, and western Mexico, which comprise the northern edge of the NAM domain. Warm SSTs on the CA margin result in greater southwesterly moisture flux and increases in precipitable water over the desert, creating a summertime energetic environment that is more favorable for moist convection. Warmer SSTs drive increases in the number of days with extreme precipitation, as well as an overall increase in summertime rainfall rates. Because SST anomalies on the CA margin show strong monthly to inter-seasonal persistence, spring or early summer SST anomalies could be used to predict years with a greater frequency of daily precipitation extremes in the northern NAM domain. Our results suggest that the extreme precipitation observed in August 2022 was at least in part modulated by the large-scale SST pattern, and that other events with similar underlying dynamics have occurred over the observational record.

The link between SSTs and NAM precipitation has been explored in previous observational and modeling studies, but results have been equivocal (Carrillo et al., 2016; Demaria et al., 2019; Griffin et al., 2013; Castro et al., 2001; Beaudin et al., 2023). This may stem from the fact that the SST pattern associated with greater daily precipitation extremes does not resemble a canonical warm ENSO or positive PDO phase. Moreover, the strongest SST-rainfall correlations occur in the northern NAM domain and are relatively weak in the core monsoon domain in western Mexico. Studies that focus on mode-based indices of the ENSO or the PDO, or analyze precipitation only in the core monsoon domain, may therefore have missed this association between SST anomalies on the CA margin and NAM rainfall. Our observational analyses support previous work emphasizing the importance of extratropical North Pacific SSTs in governing the spatial footprint of NAM precipitation (Beaudin et al., 2023; Fu et al., 2022; Bhattacharya et al., 2022).

Over the recent observational record, interannual SST variability on the CA margin has been linked to persistent multi-year marine heat waves (Meyer and Jin, 2017; Fewings and Brown, 2019). While previous work has explored the linkage between marine heat waves and winter precipitation over western North America (Swain et al., 2014), we provide an observational link between extreme events in the marine realm and extreme *summertime* precipitation on land. Given that observational data and paleoclimate records suggest strong decadal variability of CA margin SSTs, our results also raise the possibility for decadal modulation of precipitation extremes in the desert southwest (O'Mara et al., 2019). While there is some evidence for decadal variability in NAM precipitation extremes, more long-term precipitation datasets, including paleoclimate proxy datasets, are needed to explore this possibility (Demaria et al., 2019; Griffin et al., 2013).

It is possible that the strength of the CA margin SST-northern NAM domain rainfall relationship is modulated by equatorial Pacific SSTs. El Niño events result in a southward shift of the intertropical convergence zone in the EEP, enhancing atmospheric stability over the southwest (Pascale et al., 2017). In addition, central Pacific El Niño events may reduce NAM rainfall by inhibiting the development of disturbances that can serve as precursors to strong surges of NAM convection (e.g., Gulf of California surges) (Kim et al., 2011). We are unable to disentangle the relative influence of subtropical versus tropical SSTs on northern NAM precipitation in this study because of the limited observational record that offers few realizations of extreme precipitation events, especially since tropical and subtropical SST variability are highly correlated. Long integration of ESM simulations, as well as AMIP-style simulations, would be a useful next step for disentangling the importance of subtropical versus tropical SST variability on desert southwest precipitation.

Finally, we showed that historical simulations of ESMs show varying skill at reproducing the correlation between CA Margin SSTs and northern NAM precipitation. ESMs featuring a strong warm bias on the CA Margin show less skill at reproducing the observed correlation. Indeed, some ESMs produce significant correlations of the wrong sign. We hypothesize that ESMs with a strong warm bias underestimate the coupling strength of atmospheric circulation and SST on the CA margin. Both CMIP5 and CMIP6 ESMs exhibit systematic warm SST biases in the subtropical northeast Pacific, likely stemming from biases in shortwave radiation and ocean heat transport (Zhang et al., 2023; Wills et al., 2022). Given the results presented herein, many ESMs are likely to systematically misrepresent an important source of interannual variability in desert southwest precipitation. This in turn undermines confidence in studies that use direct or downscaled ESM outputs to quantify future changes in precipitation extremes, estimate signal-to-noise ratios for regional hydroclimate, or analyze future changes in hydroclimate-related risk over the desert southwest (AghaKouchak et al., 2020; Marvel et al., 2019). CMIP6 models are known to underestimate the severity and duration of multi-month or multi-year marine heat waves, similar to those that cause warming on the southern CA margin, and may contain persistent biases that influence their ability to reproduce observed SST trends (Plecha and Soares, 2020; Seager et al., 2019, 2022). Efforts to improve ESM representation of climatological SSTs and SST variability will therefore greatly improve our ability to estimate variability and trends in precipitation extremes, with broad implications for our understanding of future regional hydroclimate-related risks, especially in arid regions like the desert southwest.

It remains an open question as to whether the relationship between SSTs on the CA margin and northern NAM precipitation will persist into the 21st century. Modeling studies predict a weakening of the NAM with anthropogenic warming, in part from a dynamic response resulting in a warmer, more stable troposphere over the southwest (Pascale et al., 2017) and thus a higher threshold for convection (Pascale et al., 2018). A given CA margin SST anomaly may become less effective at generating positive anomalies of CAPE over the northern NAM domain, decreasing the correlation to summertime precipitation in this region. We briefly assess this possibility by analyzing the four ESMs that best reproduce the observed CA margin SST-northern NAM precipitation correlation, and find that all produce a strong, statistically significant correlation well into the 21st century, with two ESMs even producing a strengthening of this association (Figure S12,S13). While further analyses, especially using large ensemble approaches or AMIP-style simulations, are needed to disentangle the relative influence of interannual SST variability and forced changes on future precipitation in the northern NAM domain, our results suggest that the CA margin SST-NAM monsoon linkage could aid the effort to predict monsoon extremes well into the 21st century.

5. Acknowledgments

The authors thank John Chiang (University of California Berkeley) for valuable feedback on this work. TB acknowledges funding from NSF P2C2 Grant OCE-1903148 and OCE-2103015. RF acknowledges funding from NSF P2C2 Grant OCE-1903650 and OCE-2103055.

6. Data Availability Statement

No new data were created or analysed in this study.

7. References

References

Adams D K and Comrie A C 1997 The North American Monsoon *Bulletin of the American Meteorological Society* **78**(10), 2197–2214.

Adler R F, Sapiano M R, Huffman G J, Wang J J, Gu G, Bolvin D, Chiu L, Schneider U, Becker A, Nelkin E, Xie P, Ferraro R and Shin D B 2018 The Global Precipitation Climatology Project (GPCP) monthly analysis (new version 2.3) and a review of 2017 global precipitation *Atmosphere* **9**(4), 138.

AghaKouchak A, Chiang F, Huning L S, Love C A, Mallakpour I, Mazdiyasni O, Moftakhari H, Papalexiou S M, Ragno E and Sadegh M 2020 Climate Extremes and Compound Hazards in a Warming World *Annual Review of Earth and Planetary Sciences* **48**(1), 519–548.
URL: *https://www.annualreviews.org/doi/10.1146/annurev-earth-071719-055228*

Almazroui M, Islam M N, Saeed F, Saeed S, Ismail M, Ehsan M A, Diallo I, O'Brien E, Ashfaq M, Martínez-Castro D et al. 2021 Projected changes in temperature and precipitation over the United States, Central America, and the Caribbean in CMIP6 GCMs *Earth Systems and Environment* **5**, 1–24.

Beaudin É, Di Lorenzo E, Miller A, Seo H and Joh Y 2023 Impact of Extratropical Northeast Pacific SST on US West Coast Precipitation *Geophysical Research Letters* **50**(3), e2022GL102354.

Bhattacharya T 2022 An Energetic Perspective on the Holocene North American Monsoon *Geophysical Research Letters* **49**(19), e2022GL100782.

Bhattacharya T, Feng R, Tierney J E, Rubbelke C, Burls N, Knapp S and Fu M 2022 Expansion and intensification of the North American Monsoon during the Pliocene *AGU Advances* **3**(6), e2022AV000757.

Bieda S W, Castro C L, Mullen S L, Comrie A C and Pytlak E 2009 The relationship of transient upper-level troughs to variability of the North American monsoon system *Journal of Climate* **22**(15), 4213–4227.

Bordoni S and Stevens B 2006 Principal component analysis of the summertime winds over the Gulf of California: A gulf surge index *Monthly weather review* **134**(11), 3395–3414.

Canon G 2022 Record Death Valley flooding 'a once-in-1,000-year event' *The Guardian* . **URL:** *https://www.theguardian.com/us-news/2022/aug/10/death-valley-floods-climate-crisis*

Capotondi A, Newman M, Xu T and Di Lorenzo E 2022 An optimal precursor of Northeast Pacific marine heatwaves and Central Pacific El Niño events *Geophysical Research Letters* **49**(5), e2021GL097350.

Carrillo C M, Castro C L, Woodhouse C A and Griffin D 2016 Low-frequency variability of precipitation in the North American Monsoon region as diagnosed through earlywood and latewood tree-ring chronologies in the southwestern US *International Journal of Climatology* **36**(5), 2254–2272.

Castro C L, McKee T B and Pielke R A 2001 The relationship of the North American monsoon to tropical and North Pacific sea surface temperatures as revealed by observational analyses *Journal of Climate* **14**(24), 4449–4473.

Cavazos T, Turrent C and Lettenmaier D 2008 Extreme precipitation trends associated with tropical cyclones in the core of the North American monsoon *Geophysical Research Letters* **35**(21).

Chang P, Zhang S, Danabasoglu G, Yeager S G, Fu H, Wang H, Castruccio F S, Chen Y, Edwards J, Fu D et al. 2020 An unprecedented set of high-resolution earth system simulations for understanding multiscale interactions in climate variability and change *Journal of Advances in Modeling Earth Systems* **12**(12), e2020MS002298.

Clemesha R E, Iacobellis S F, Gershunov A, Cayan D R, Small I J and Cavazos T 2023 North American monsoon impacts southern California's coastal low clouds *Geophysical Research Letters* **50**(12), e2022GL102059.

Coats S, Smerdon J E, Seager R, Griffin D and Cook B I 2015 Winter-to-summer precipitation phasing in southwestern North America: A multicentury perspective from paleoclimatic model-data comparisons *Journal of Geophysical Research: Atmospheres* **120**(16), 8052–8064.

Cook B I and Seager R 2013 The response of the North American Monsoon to increased greenhouse gas forcing *Journal of Geophysical Research: Atmospheres* **118**(4), 1690–1699.

Demaria E M, Hazenberg P, Scott R L, Meles M B, Nichols M and Goodrich D 2019 Intensification of the North American Monsoon rainfall as observed from a long-term high-density gauge network *Geophysical Research Letters* **46**(12), 6839–6847.

Di Lorenzo E, Xu T, Zhao Y, Newman M, Capotondi A, Stevenson S, Amaya D, Anderson B, Ding R, Furtado J et al. 2023 Modes and mechanisms of pacific decadal-scale variability *Annual Review of Marine Science* **15**, 249–275.

Eyring V, Bony S, Meehl G A, Senior C A, Stevens B, Stouffer R J and Taylor K E 2016 Overview of the Coupled Model Intercomparison Project Phase 6 (CMIP6) experimental design and organization *Geoscientific Model Development* **9**(5), 1937–1958.

Fewings M R and Brown K S 2019 Regional structure in the marine heat wave of summer 2015 off the western United States *Frontiers in Marine Science* **6**, 564.

Fu M, Cane M A, Molnar P and Tziperman E 2022 Warmer Pliocene upwelling site SST leads to wetter subtropical coastal areas: A positive feedback on SST *Paleoceanography and Paleoclimatology* **37**(2), e2021PA004357.

Griffin D, Woodhouse C A, Meko D M, Stahle D W, Faulstich H L, Carrillo C, Touchan R, Castro C L and Leavitt S W 2013 North American monsoon precipitation reconstructed from tree-ring latewood *Geophysical Research Letters* **40**(5), 954–958.

Haarsma R J, Roberts M J, Vidale P L, Senior C A, Bellucci A, Bao Q, Chang P, Corti S, Fučkar N S, Guemas V et al. 2016 High resolution model intercomparison project (HighResMIP v1. 0) for CMIP6 *Geoscientific Model Development* **9**(11), 4185–4208.

Ishii M, Shouji A, Sugimoto S and Matsumoto T 2005 Objective analyses of sea-surface temperature and marine meteorological variables for the 20th century using ICOADS and the Kobe collection *International Journal of Climatology: A Journal of the Royal Meteorological Society* **25**(7), 865–879.

Johnson B O and Delworth T L 2023 The Role of the Gulf of California in the North American Monsoon *Journal of Climate* **36**(6), 1541–1559.

Kalnay E, Kanamitsu M, Kistler R, Collins W, Deaven D, Gandin L, Iredell M, Saha S, White G, Woollen J, Zhu Y, Chelliah M E, Higgins W, Janowiak J, Mo K, Ropelewski C, Wang J, Leetmaa A, Reynolds R, Jenne R and Joseph D 1996 The NCEP/NCAR 40-year reanalysis project *Bulletin of the American meteorological Society* **77**(3), 437–472.

Kim H M, Webster P J and Curry J A 2011 Modulation of North Pacific tropical cyclone activity by three phases of ENSO *Journal of Climate* **24**(6), 1839–1849.

Liebmann B and Smith C A 1996 Description of a complete (interpolated) outgoing longwave radiation dataset *Bulletin of the American Meteorological Society* **77**(6), 1275–1277.

Marvel K, Cook B I, Bonfils C J, Durack P J, Smerdon J E and Williams A P 2019 Twentieth-century hydroclimate changes consistent with human influence *Nature* **569**(7754), 59–65.

Mazon J J, Castro C L, Adams D K, Chang H I, Carrillo C M and Brost J J 2016 Objective climatological analysis of extreme weather events in Arizona during the North American monsoon *Journal of Applied Meteorology and Climatology* **55**(11), 2431–2450.

Mesinger F, DiMego G, Kalnay E, Mitchell K, Shafran P C, Ebisuzaki W, Jović D, Woollen J, Rogers E, Berbery E H, Ek M B, Fan Y, Grumbine R, Higgins W, Li H, Lin Y, Manikin G, Parrish D and Shi W 2006 North American regional reanalysis *Bulletin of the American Meteorological Society* **87**(3), 343–360.

Meyer J D and Jin J 2017 The response of future projections of the North American monsoon when combining dynamical downscaling and bias correction of CCSM4 output *Climate Dynamics* **49**(1-2), 433–447.

Moloney K A, Mudrak E L, Fuentes-Ramirez A, Parag H, Schat M and Holzapfel C 2019 Increased fire risk in Mojave and Sonoran shrublands due to exotic species and extreme rainfall events *Ecosphere* **10**(2), e02592.

Moon S and Ha K J 2020 Future changes in monsoon duration and precipitation using CMIP6 *npj Climate and Atmospheric Science* **3**(1), 45.

O'Mara N A, Cheung A H, Kelly C S, Sandwick S, Herbert T D, Russell J M, Abella-Gutiérrez J, Dee S G, Swarzenski P W and Herguera J C 2019 Subtropical Pacific Ocean Temperature Fluctuations in the Common Era: Multidecadal Variability and Its Relationship With Southwestern North American Megadroughts *Geophysical Research Letters* **46**(24), 14662–14673.
URL: *https://onlinelibrary.wiley.com/doi/10.1029/2019GL084828*

O'Gorman P A 2015 Precipitation Extremes Under Climate Change *Current Climate Change Reports* **1**(2), 49–59.
URL: *http://link.springer.com/10.1007/s40641-015-0009-3*

Pascale S, Boos W R, Bordoni S, Delworth T L, Kapnick S B, Murakami H, Vecchi G A and Zhang W 2017 Weakening of the North American monsoon with global warming *Nature Climate Change* **7**(11), 806–812.

Pascale S, Bordoni S, Kapnick S B, Vecchi G A, Jia L, Delworth T L, Underwood S and Anderson W 2016 The impact of horizontal resolution on North American Monsoon Gulf of California moisture surges in a suite of coupled global climate models *Journal of Climate* **29**(21), 7911–7936.

Pascale S, Kapnick S B, Bordoni S and Delworth T L 2018 The influence of CO2 forcing on North American monsoon moisture surges *Journal of Climate* **31**(19), 7949–7968.

Plecha S M and Soares P M 2020 Global marine heatwave events using the new CMIP6 multi-model ensemble: from shortcomings in present climate to future projections *Environmental Research Letters* **15**(12), 124058.

Ren X, Liu W, Capotondi A, Amaya D J and Holbrook N J 2023 The Pacific Decadal Oscillation modulated marine heatwaves in the Northeast Pacific during past decades *Communications Earth & Environment* **4**(1), 218.

Schneider U, Fuchs T, Meyer-Christoffer A and Rudolf B 2008 Global precipitation analysis products of the GPCC *Global Precipitation Climatology Centre (GPCC), DWD, Internet Publikation* **112**.

Seager R, Cane M, Henderson N, Lee D E, Abernathey R and Zhang H 2019 Strengthening tropical Pacific zonal sea surface temperature gradient consistent with rising greenhouse gases *Nature Climate Change* **9**(7), 517–522.

Seager R, Henderson N and Cane M 2022 Persistent discrepancies between observed and modeled trends in the tropical Pacific Ocean *Journal of Climate* **35**(14), 4571–4584.

Seager R, Murtugudde R, Naik N, Clement A, Gordon N and Miller J 2003 Air–sea interaction and the seasonal cycle of the subtropical anticyclones *Journal of climate* **16**(12), 1948–1966.

Sillmann J, Kharin V, Zhang X, Zwiers F and Bronaugh D 2013 Climate extremes indices in the CMIP5 multimodel ensemble: Part 1. Model evaluation in the present climate *Journal of geophysical research: atmospheres* **118**(4), 1716–1733.

Swain D L, Tsiang M, Haugen M, Singh D, Charland A, Rajaratnam B and Diffenbaugh N S 2014 The extraordinary California drought of 2013/2014: Character, context, and the role of climate change *Bulletin of the American Meteorological Society* **95**(9), S3.

Varuolo-Clarke A M, Reed K A and Medeiros B 2019 Characterizing the North American monsoon in the Community Atmosphere Model: Sensitivity to resolution and topography *Journal of Climate* **32**(23), 8355–8372.

Wei X, Li K Y, Kilpatrick T, Wang M and Xie S P 2021 Large-scale conditions for the record-setting Southern California marine heatwave of August 2018 *Geophysical Research Letters* **48**(7), e2020GL091803.

Wilks D S 2011 *Statistical Methods in the Atmospheric Sciences* Vol. 100 Academic press.

Wills R C, Dong Y, Proistosecu C, Armour K C and Battisti D S 2022 Systematic Climate Model Biases in the Large-Scale Patterns of Recent Sea-Surface Temperature and Sea-Level Pressure Change *Geophysical Research Letters* **49**(17), e2022GL100011.

Xie P, Arkin P A and Janowiak J E 2007 CMAP: The CPC merged analysis of precipitation *Measuring precipitation from space* **28**, 319–328.

Yang L, Smith J, Baeck M L, Morin E and Goodrich D C 2017 Flash flooding in arid/semiarid regions: Dissecting the hydrometeorology and hydrology of the 19 August 2014 storm and flood hydroclimatology in Arizona *Journal of Hydrometeorology* **18**(12), 3103–3123.

Zhang Q, Liu B, Li S and Zhou T 2023 Understanding Models' Global Sea Surface Temperature Bias in Mean State: From CMIP5 to CMIP6 *Geophysical Research Letters* **50**(4).
URL: *https://onlinelibrary.wiley.com/doi/10.1029/2022GL100888*

8. Figures and Figure Captions

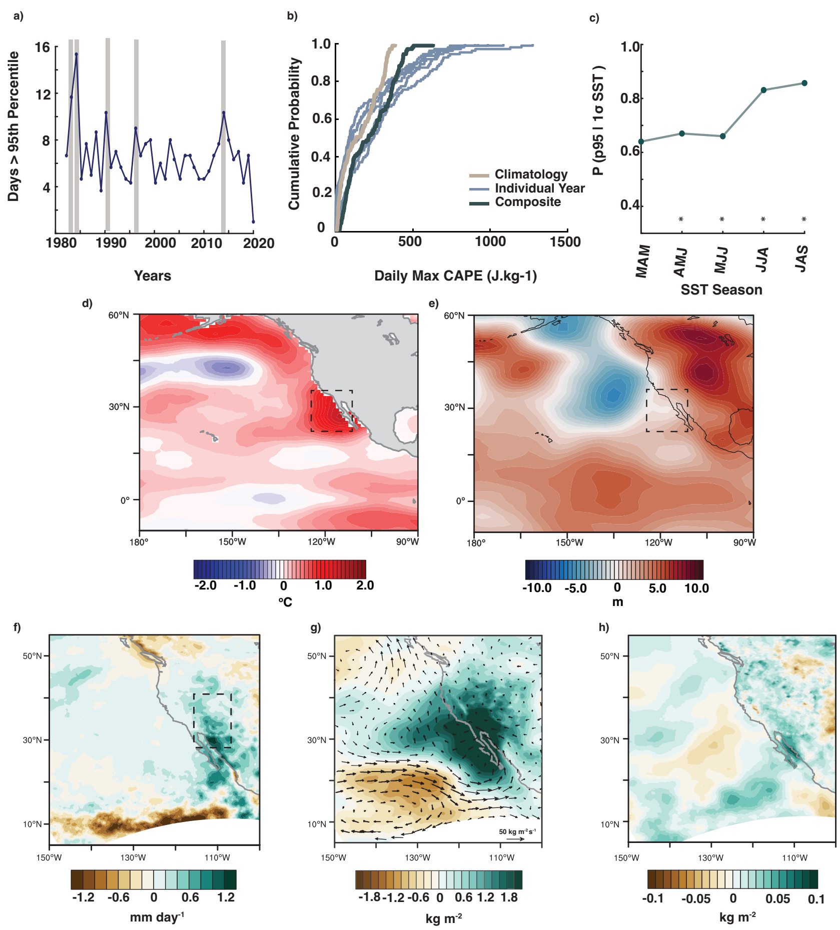

Figure 1. Composites associated with summers featuring the greatest number of extreme precipitation days. a) number of summertime days with precipitation exceeding the 95th percentile (p95) between 1981 and 2020 over the region between 28 and 37 °N and 115 and 108 °W (this region is outlined in box in panel f). Gray bars highlight the five years with the greatest number of extreme precipitation days (1983, 1984, 1990, 1996, and 2014). b) daily maximum of 3-hourly CAPE for climatology (tan), each individual summer (light blue) and a composite of all summers (dark blue). c) probability of seeing greater than 6 days of precipitation above p95 between July and September in the presence of a warm SST anomaly on the CA margin at different leading seasons. Seasons with $*$ are statistically significant at the 95% level. d) and e) SST and 850-mb geopotential height composite anomaly associated with these five summers, with box showing region used for SST index in subsequent figures. f) monthly-mean NARR rainfall composite during these summers; g) Anomalies of vertically integrated moisture flux (vectors) and total precipitable water (shading); h) evaporation composite anomaly (shading).

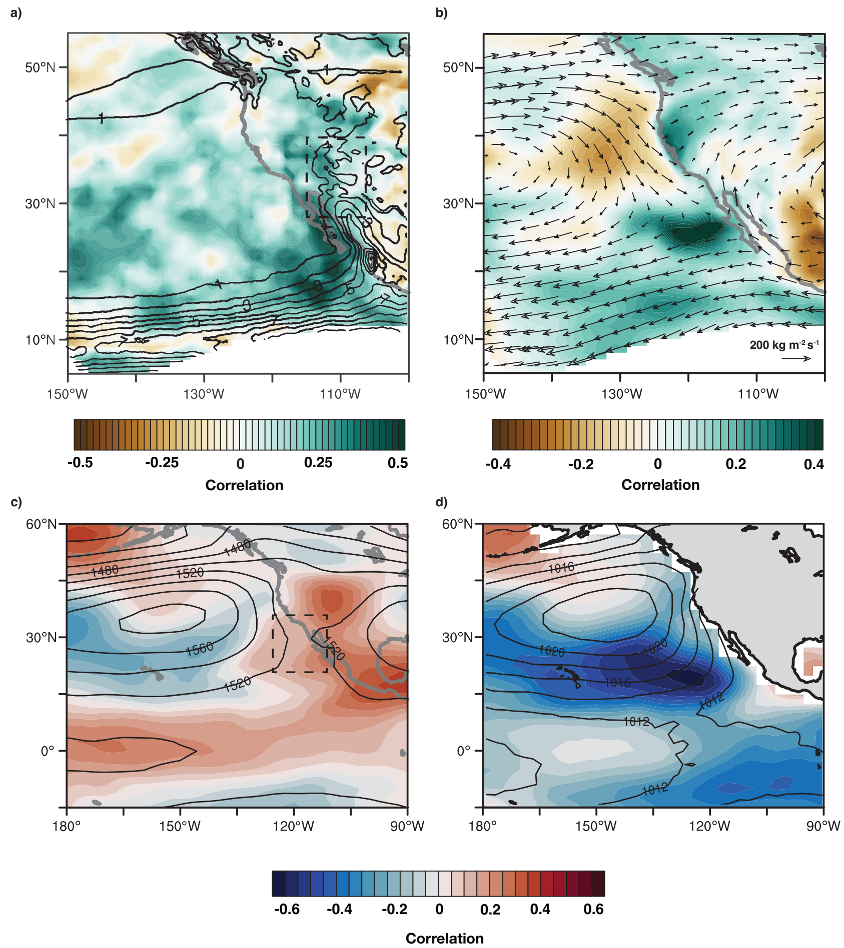

Figure 2. Correlation between southern CA margin SSTs over region shown in dashed box (25 to 32 °N and 125 to 110 °W) and hydroclimate. a) correlation between precipitation in NARR and SST index (shading) superimposed on climatological contours of precipitation (contours). b) Climatological vertically integrated zonal and meridional moisture flux (vectors) with correlation between meridional moisture flux and SST index (shading). c) Climatological 850 mb geopotential height (contours), superimposed on correlation between 850 mb geopotential heights and SST index (shading). d) Climatological SLP (contours) and SLP-SST index correlation (shading).

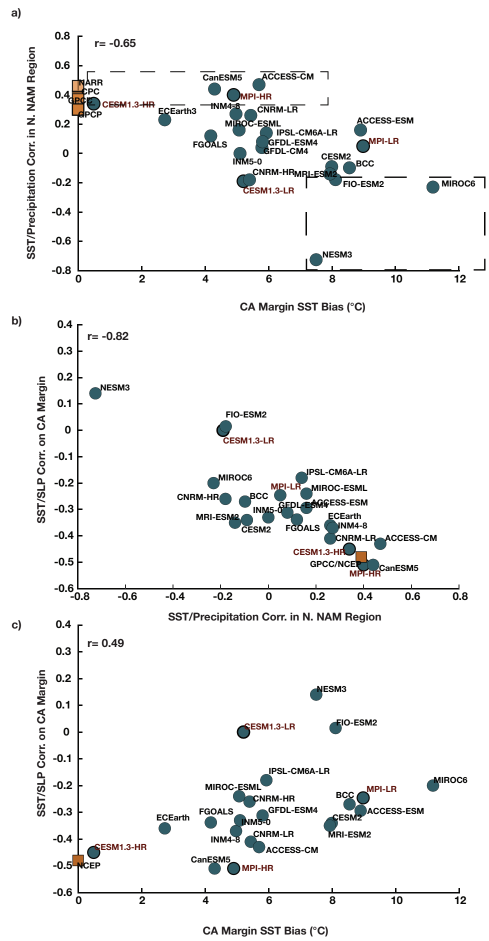

Figure 3. Relationship between SST bias and hydroclimate in observational products compared to CMIP5 and CMIP6 ESMs. a) Scatterplot of SST bias over 25 and 32 °N and 125 and 110 °W on the CA margin (x axis), and the strength of the correlation between SSTs in this region and precipitation in the northern NAM domain (27 and 37 °N and 115 and 107 °W–y axis). Subsets of ESMs used in Figure 4 outlined in dashed rectangles. b) Relationship between the strength of precipitation-SST correlation shown in panel a (x axis) and the correlation between SLP (20 and 30 °N and 125 and 110 °W) and SST over CA margin (y axis); c) Relationship between SST bias on the CA margin (x axis) and the SLP-SST correlation shown in panel b (y axis).

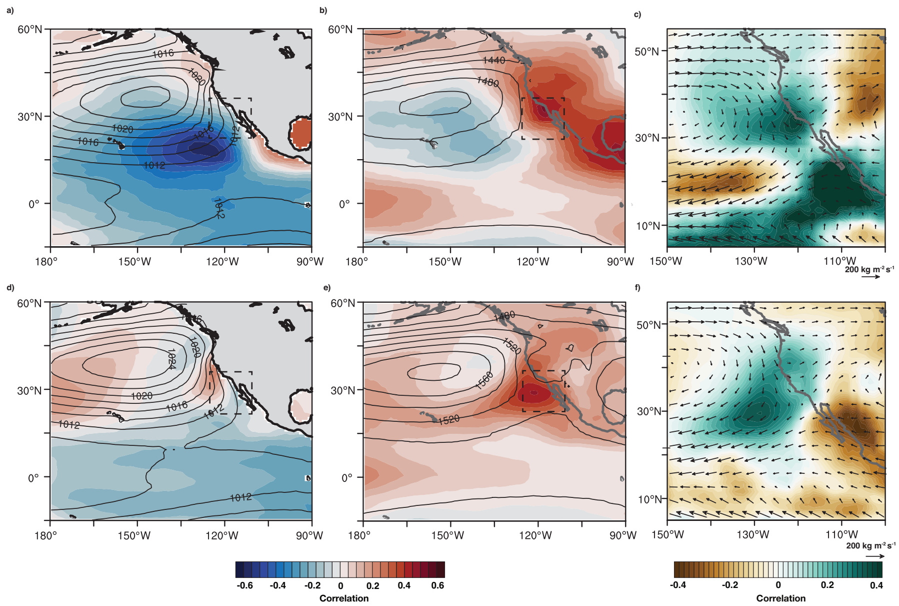

Figure 4. Contrasting relationship between large-scale climate fields and SST in ESMs that perform well (a-c) and ESMs that perform poorly (d-f) at reproducing the SST-precipitation relationship. SST index calculated from the dashed box. a) and d) show climatological SLP (contours) and correlation between SLP and the SST index (shading). b) and e) as in panels a) and d) but for 850 mb geopotential height. c) and f) show climatological vertically integrated moisture flux (vectors) and correlation between meridional moisture flux and the SST index (shading).

Supplemental Information for *California Margin temperatures modulate extreme summer precipitation in the desert Southwest*

Tripti Bhattacharya[1], Ran Feng[2], Christopher R. Maupin[3], Sloan Coats[4], Peter R. Brennan[1], and Elizabeth Carter[5]

[1]Department of Earth and Environmental Sciences, Syracuse University, Syracuse, NY, USA

[2]Department of Geosciences, University of Connecticut, Storrs, CT, USA

[3]Department of Geography, Texas A&M University, College Station, TX, USA

[4]Department of Earth Sciences, University of Hawai'i at Manoa, Honolulu, HI, USA

[5]Civil and Environmental Engineering, Syracuse University, Syracuse, NY USA

September 20, 2023

Contents of this file

Text S1. Additional Methods Description

Correlation and Running Correlation Analysis

To identify the link between CA margin SSTs and monthly mean precipitation over the northern NAM domain, we calculated an index of SSTs between 25 and 32 °N and 125 and 110 °W. We then calculated the linear correlation of this index and monthly mean precipitation fields from the 0.25 °Global Precipitation Climatology Centre (GPCC) product between 1960 and 2014, the Climate Prediction Center merged analysis of precipitation (CPC), the Global Precipitation Climatology Project (GPCP), and the NARR (*Schneider et al.*, 2008; *Xie et al.*, 2007; *Adler et al.*, 2018; *Mesinger et al.*, 2006). Using multiple precipitation products helps establish the robustness of the relationship. We also evaluated the correlation between this SST index and monthly mean fields of SLP, precipitable water, and moisture flux from the NARR.

For our analysis of correlations between CA margin SSTs and precipitation across a range of Coupled Model Intercomparison Project (CMIP) phase 5 and 6 ESMs, we use an index of precipitation over land areas between 27 and 37 °N and 115 and 107 °W. For the SST-sea level pressure (SLP) correlation analysis, we use an index of SLP over ocean areas between 20 and 30 °N and 125 and 110 °W. Slight changes to the bounds of these index regions do not alter our results or conclusions.

In Figure **S13**, we plot the running correlation between CA margin SST anomalies and precipitation in future emission scenarios for the 4 ESMs that show the greatest fidelity over the historical period at producing the observed SST-precipitation correlation (high resolution configurations of CESM1.3, MPI-ESM1-2, as well as ACCESS-CM and CanESM5). This running correlation is performed in 40-year averaging windows for historical simulations, Shared Socioeconomic Pathway (SSP) 3-7.0 and 5-8.5 in the case of the MPI, ACCESS and CanESM5 ESMs, and for Representative Concentration Pathway (RCP) 8.5 in the case of CESM1.3-HR (see Table S1 for more details). Because the forcing datasets differ across these simulations, the purpose of this analysis is not to analyze the particular trajectory of NAM precipitation and SST in a given ESM versus another, although we show this in Figure **S12**. Instead, the goal of this analysis is show that the strength of the correlation between CA margin SSTs and northern NAM precipitation remains statistically significant in the future.

Contrasting Models with High and Low Skill

Figure 4 in the main text contrasts models with high and low skill at reproducing the SST-monsoon linkage (e.g. the correlation between CA margin SSTs averaged between 25 and 32 °N and 125 and 110 °W and NAM precipitation). To create composite correlation plots contrasting the best and worst models, each models' fields of 850 mb geopotential height, sea level pressure, zonal and meridional moisture flux (calculated from inputs of u and v winds as well as humidity), and precipitation from historical simulations were regridded to a common 1 °by 1 °latitude and longitude grid. We used these regridded model fields to calculate the correlation between the timeseries of each models' CA margin SST index and that models' timeseries of geopotential height, sea level pressure, moisture flux, and precipitation. Correlation fields from the good models (e.g. CESM1.3; MPI-ESM-1-2-HR; ACCESS-CM2; CanESM5-1) are averaged together to generate a 'composite' correlation field representing the good models. Similarly, climatologies of each variable from each model are computed and then averaged together to create a composite climatology for these 'good models.' These results are presented in Figure 4 in the main text and Figure S7. The same procedure is repeated for the worst performing models (e.g. NESM3; FIO-ESM2; MIROC6) to create a composite of worst-performing models.

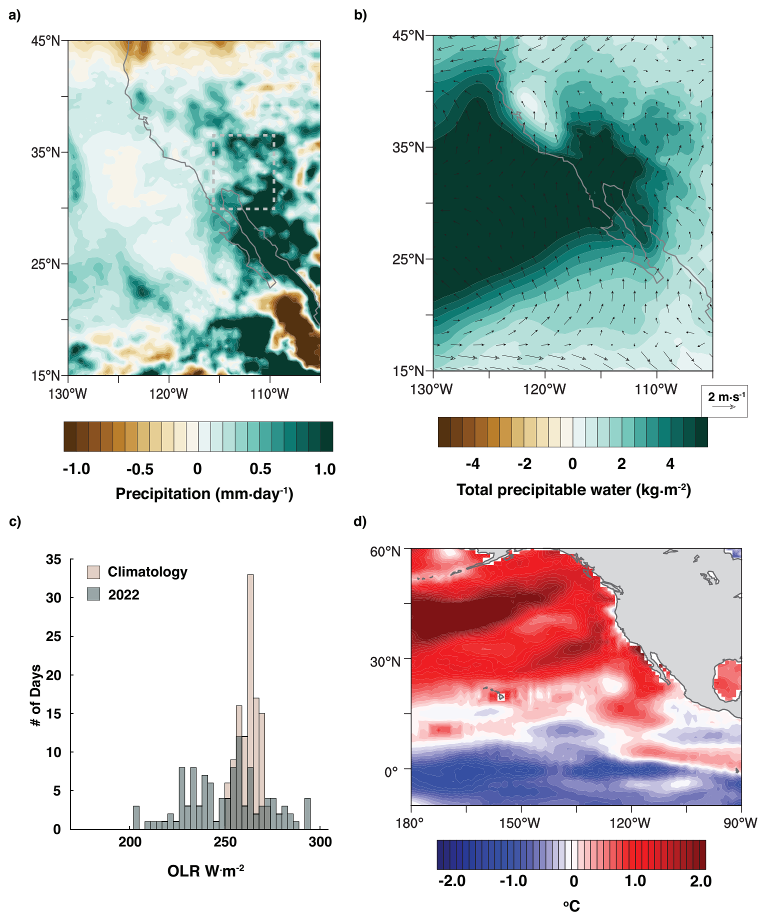

Figure S1: **Shifts in monsoon precipitation rates in summer 2022.** a) shows July-September monthly mean precipitation anomalies in mm/day. Gray box highlights the northern NAM region used for averaging, and includes Death Valley, CA. b) shows anomalies of total precipitable water and 850 mb winds. c) shows differences in daily values of outgoing longwave radiation (OLR) for summer 2022 (mint green) compared to the climatology between 1974 and 2022 (tan). The distribution of OLR for 2022 is significantly different from the climatological distribution at the 95% level according to a 2-sided Kolmogorov-Smirnov (K-S) test. d) shows summer 2022 SST anomalies in °C relative to a 1950-2022 climatology.

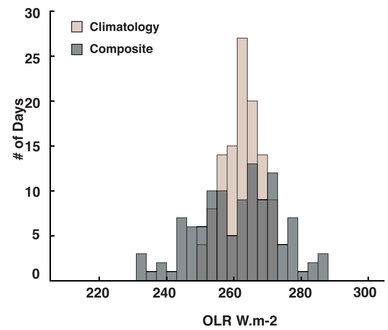

Figure S2: Differences in daily values of outgoing longwave radiation (OLR) for five summers with the greatest extreme precipitation days (mint green) compared to the climatology between 1974 and 2022 (tan). The distribution of OLR for extreme precipitation years is significantly different from the climatological distribution at the 95% level according to a 2-sided Kolmogorov-Smirnov (K-S) test.

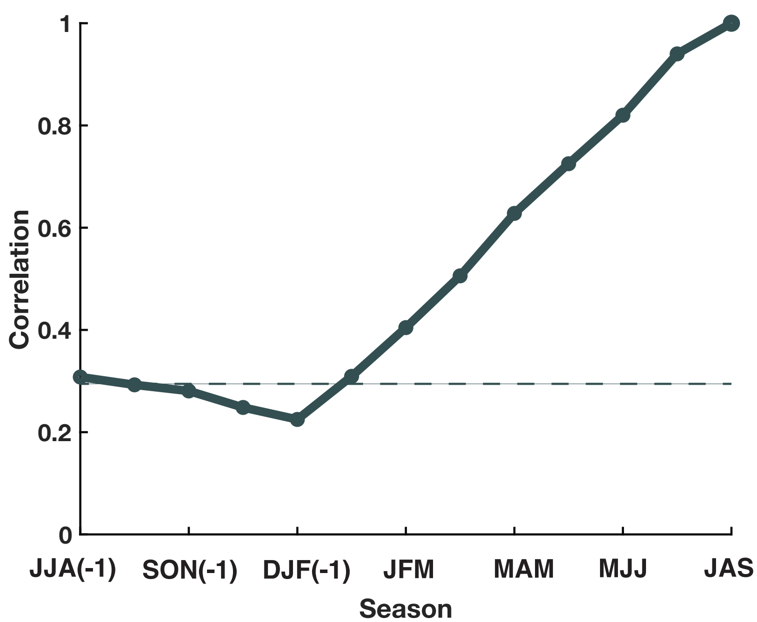

Figure S3: Correlation between July-September (JAS) SST anomalies on the CA Margin (25 and 32 °N and 125 and 110 °W) and simultaneous (JAS) and prior seasons' SST anomalies, starting with JJA, then MJJ, AMJ, MAM, etc. until JJA in the prior year. Significance of correlation level is indicated by the dashed line.

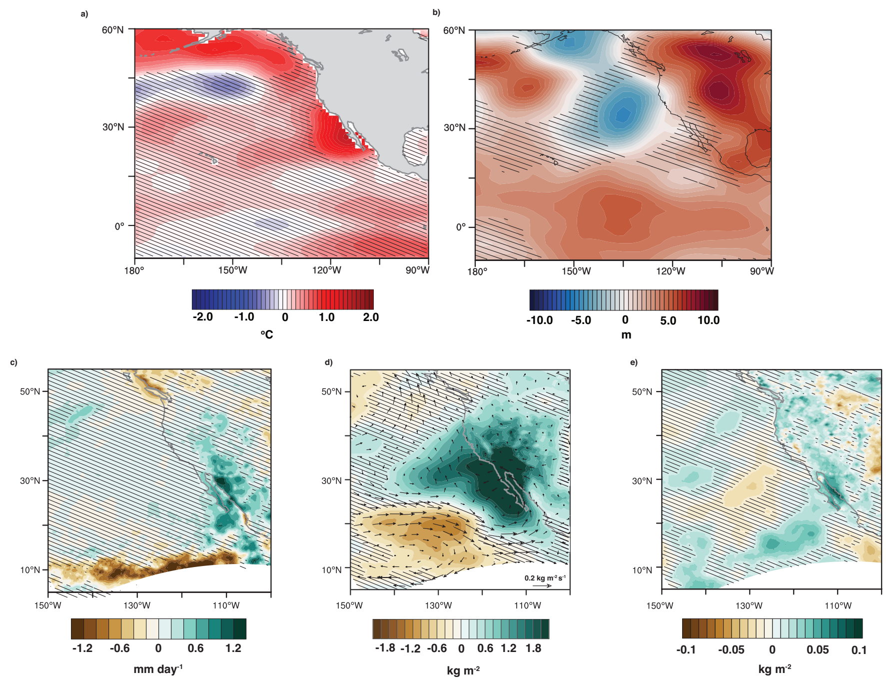

Figure S4: Fields shown in Figure 1 in main text, with shading to indicate regions where composite anomalies are not statistically significant. a) SST; b) 850 mb geopotential height; c) NARR monthly mean precipitation rate d) moisture flux and total precipitable water (shading indicates significance of precipitable water composite anomalies). e) evaporation. Significance determined via a two-sided t-test.

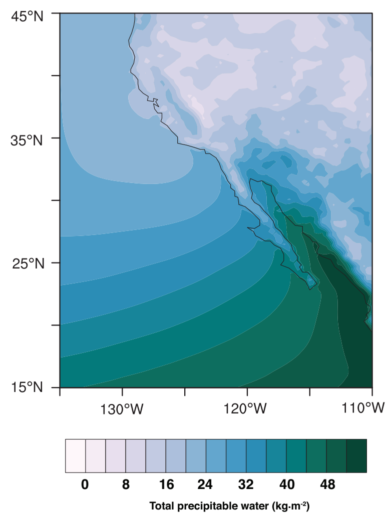

Figure S5: July-September climatology of total precipitable water in kg/m^2 over the southwest US and western Mexico. Data from the North American Regional Reanalysis (*Mesinger et al.*, 2006). Climatology shows strong gradients from 30-40 °N, where there are very low values of precipitable water over desert regions of the southwest.

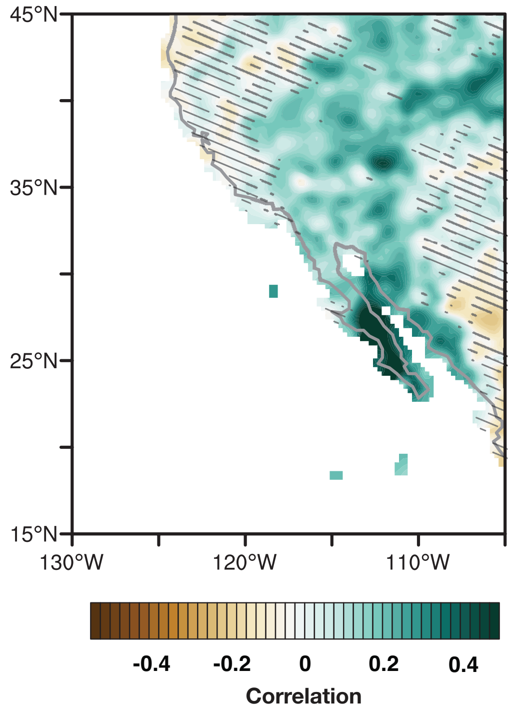

Figure S6: Correlation between CA Margin SSTs and GPCC precipitation in GPCC precipitation. SSTs are an index between 25 and 32 °N and 125 and 110 °W, taken from the COBE SST product (*Ishii et al.*, 2005). Shading indicates regions where correlation is not statistically significant. See next figure for correlation with multiple products

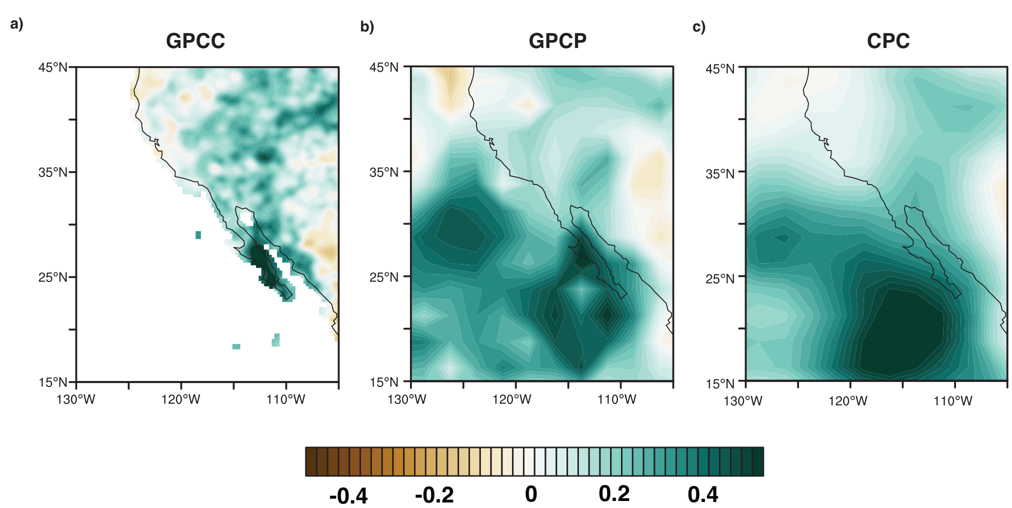

Figure S7: Correlation between CA Margin SSTs and precipitation in multiple products. SSTs are an index between 25 and 32 °N and 125 and 110 °W, taken from the COBE SST product (*Ishii et al.*, 2005).

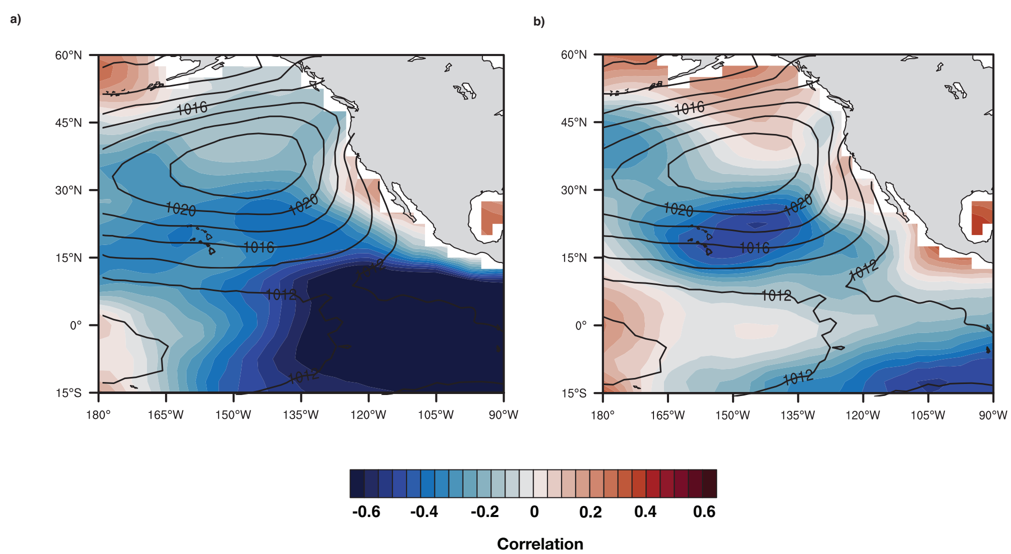

Figure S8: Correlation between sea level pressure (SLP) over the northeast Pacific and other modes of variability. a) shows simultaneous correlation between Niño 3.4 index and SLP; b) shows simultaneous correlation between the Pacific Decadal Oscillation (PDO) and SLP. Solid contours represent climatological values of SLP

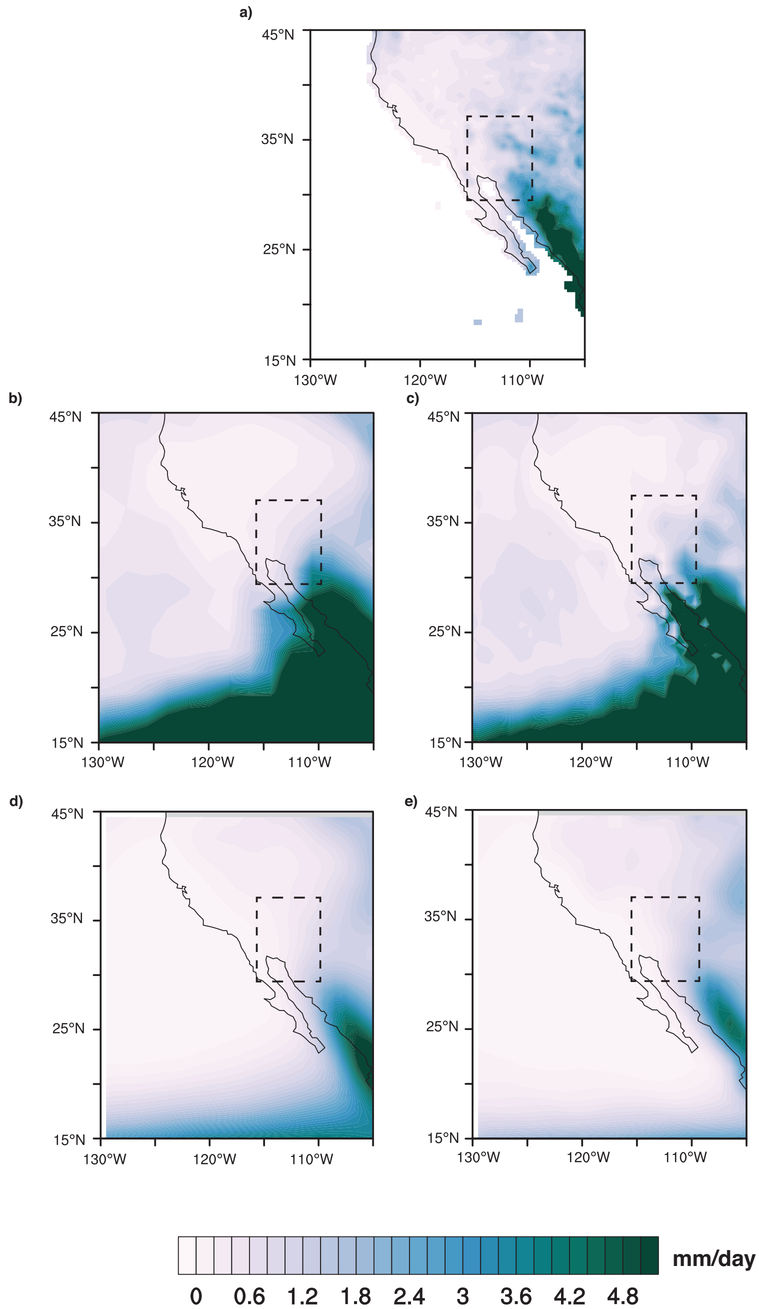

Figure S9: July-September climatology of low vs. high resolution ESMs. a) shows observational climatology of summertime precipitation from the GPCC 0.25 °product; b) shows MPI-ESM1-2 low resolution summertime rainfall climatology; c) shows MPI-ESM1-2 high resolution climatology; d) shows CESM1.3 low resolution climatology; e) shows CESM1.3 high resolution climatology. All ESM climatologies are computed from 1950-2014 in historical simulations. Dashed box outlines the region used for precipitation averages shown in Figure 5 in the main text. Climatologies of rainfall rates show only a small improvement over this dashed box in the high resolution version of the ESMs

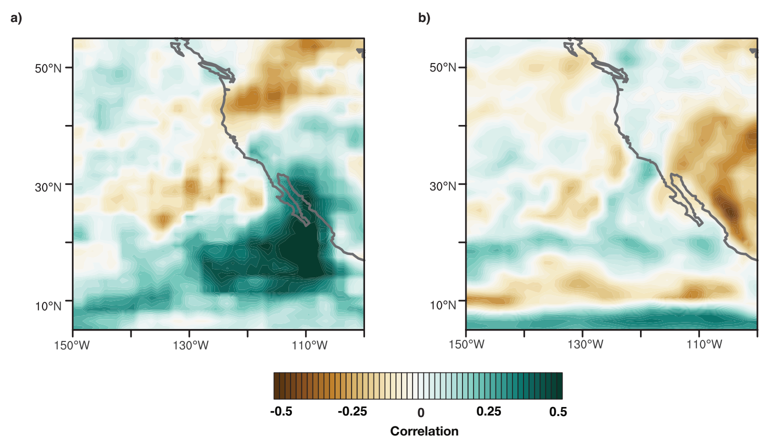

Figure S10: July-September correlation of precipitation with CA margin SST anomalies (see text for index definition) contrasting models that perform well and those that perform poorly. a) shows models with good skill at reproducing SST-monsoon linkage (CESM1.3; ACCESS-CM2; CanESM5-1; MPI-ESM-1-2-HR) and b) shows model with poor skill at simulating linkage (FIO-ESM-2; NESM3; MIROC6).

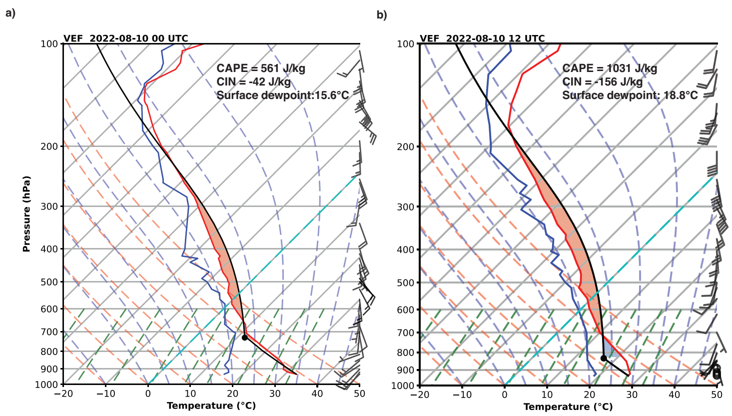

Figure S11: Las Vegas (VEF) observed soundings, 10 August 2022 at a) 00Z and b) 12Z. Atmospheric temperature (red), dewpoint temperature (blue) and windspeed with direction (barbs) shown as a function of atmospheric pressure. Profiles (black line) are calculated by dry adiabatic lifting of parcels to the lifted condensation level (LCL, filled black circle). Convective inhibition (CIN; blue shading) and convective available potential energy (CAPE; red shading) are calculated from the surface to the LCL, and from the surface to the equilibrium level (EL), respectively. Both soundings document nearly identical precipitable water amounts, despite a nearly twofold jump in CAPE within 12 hours. The increase in instability is associated with a turning of the low-level winds from southwesterly to southerly. A corresponding moistening from the surface to 700 hPa from this southerly transport, visible when comparing sounding dewpoint temperatures, lowers the LCL, contributing to the strong increase in instability and CAPE.

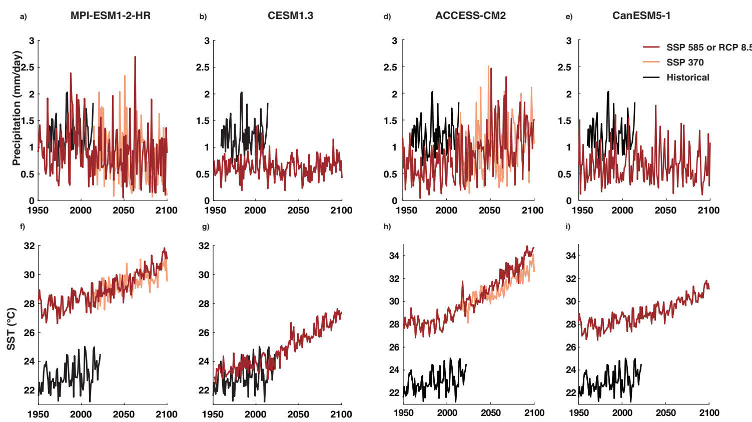

Figure S12: 21st century changes in precipitation and SST for ESMs that exhibit CA margin SST-northern NAM rainfall correlations similar to observations. Top panel shows precipitation (mm/day); bottom panel shows SST (°C). a) and f) are MPI-ESM1-2; b) and g) are CESM1.3; c) and h) are ACCESS-CM2; and d) and i) are CanESM5-1. SSTs and precipitation are in absolute units rather than anomalies in order to highlight SST and precipitation biases.

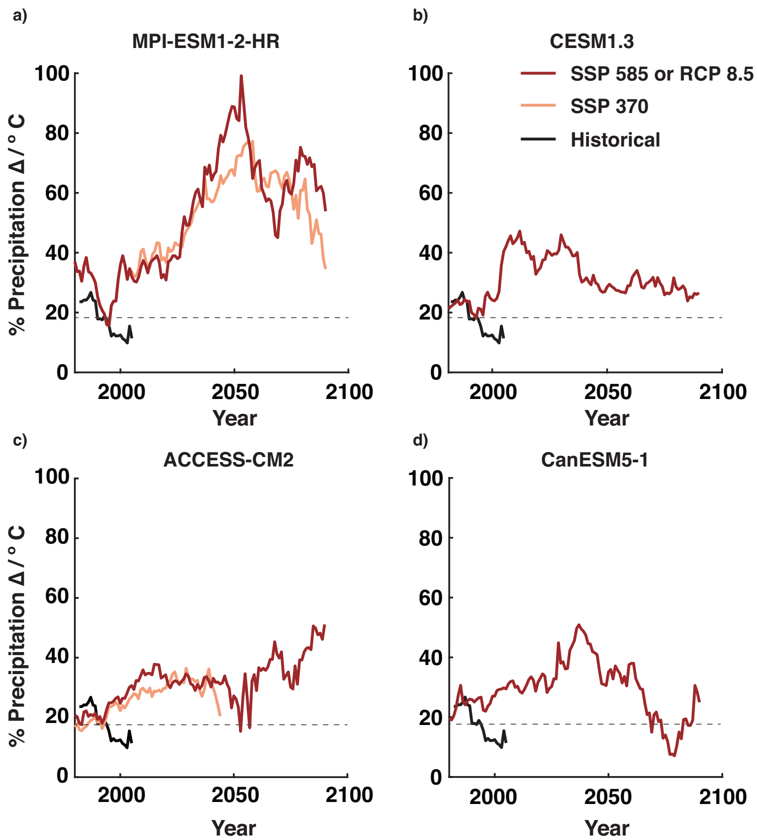

Figure S13: Running correlation between CA margin SST and precipitation for future emissions scenarios across four ESMs that show the highest skill at reproducing the observed SST-precipitation correlation (see Figure 4 in main text). Correlations above the dashed line are statistically significant at the 95% level.

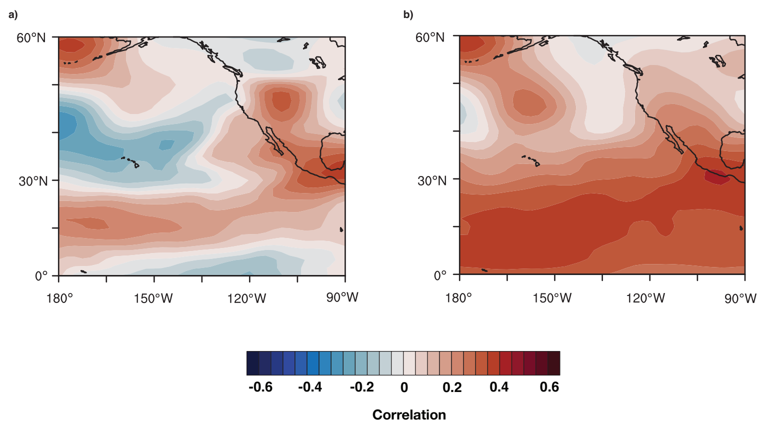

Figure S14: Contrasting correlation patterns between geopotential height and CA margin SST index in NCEP-NCAR reanalysis. a) shows 850 mb heights (similar to the pattern in Figure 2 in the main text); b) shows 500 mb height pattern.

Table S1: CMIP6 and CMIP5 models used to analyze the relationship between SST bias between 22 and 30 °N and 125 and 110 °W, on the CA margin, and the relationship between SSTs, precipitation, and SLP over northern NAM domain shown in Figure 4 and Figure 5 in the main text. Acronym refers to the acronym used in Figure 4 in the main text.

Institution	Model Name	Acronym	Simulations Analyzed
National Center for Atmospheric Research	CESM2	CESM2	CMIP6 historical
National Center for Atmospheric Research	CESM1.3 low-res	CESM1.3 LR	CMIP5 historical
National Center for Atmospheric Research	CESM1.3 high-res	CESM1.3 HR	CMIP5 historical RCP8.5
EC Earth Consortium	EC-Earth3	ECEarth3	CMIP6 historical
Model for Interdisciplinary Research on Climate	MIROC6	MIROC6	CMIP6 historical
Model for Interdisciplinary Research on Climate	MIROC-ESM2-L	MIROC-ESML	CMIP6 historical
Geophysical Fluid Dynamics Laboratory	GFDL-CM4	GFDL-CM4	CMIP6 historical
Geophysical Fluid Dynamics Laboratory	GFDL-ESM4	GFDL-ESM4	CMIP6 historical
L'Institut Pierre-Simon Laplace	IPSL-CM6A-LR	IPSL-CM6A-LR	CMIP6 historical
Beijing Climate Center	BCC-CSM2-MR	BCC	CMIP6 historical
State Key Laboratory of Numerical Modeling for Atmospheric Sciences and Geophysical Fluid Dynamics	FGOALS-g3	FGOALS	CMIP6 historical
Max Planck Institute for Meteorology	MPI-ESM1-2-LR	MPI-LR	CMIP6 historical
Max Planck Institute for Meteorology	MPI-ESM1-2-HR	MPI-HR	CMIP6 historical SSP585 SSP370
Canadian Centre for Climate Modelling and Analysis	CanESM5-1	CanESM5	CMIP6 historical SSP585
Centre National de Recherches Météorologiques	CNRM-CM6-1	CNRM-LR	CMIP6 historical
Centre National de Recherches Météorologiques	CNRM-CM6-1	CNRM-HR	CMIP6 historical
Commonwealth Scientific & Industrial Research Organisation Australia	ACCESS-CM2	ACCESS-CM	CMIP6 historical SSP585 SSP370
Commonwealth Scientific and Industrial Research Organisation Australia	ACCESS-ESM2	ACCESS-ESM	CMIP6 historical
Nanjing University of Information Science and Technology China	NESM3	NESM3	CMIP6 historical
First Institute of Oceanography and Pilot National Laboratory for Marine Science and Technology	FIO-ESM2	IO-ESM2	CMIP6 historical
Meteorological Research Institute Japan	MRI-ESM-2.0	MRI-ESM2	CMIP6 historical
Institute for Numerical Mathematics Russian Federation	INM-CM4-8	INM4-8	CMIP6 historical
Institute for Numerical Mathematics Russian Federation	INM-CM5-0	INM5-0	CMIP6 historical

References

Adams, D. K., and A. C. Comrie (1997), The north american monsoon, *Bulletin of the American Meteorological Society*, *78*(10), 2197–2214.

Adams, J. L., and D. J. Stensrud (2007), Impact of tropical easterly waves on the North American monsoon, *Journal of climate*, *20*(7), 1219–1238.

Adler, R. F., M. R. Sapiano, G. J. Huffman, J.-J. Wang, G. Gu, D. Bolvin, L. Chiu, U. Schneider, A. Becker, E. Nelkin, P. Xie, R. Ferraro, and D.-B. Shin (2018), The global precipitation climatology project (gpcp) monthly analysis (new version 2.3) and a review of 2017 global precipitation, *Atmosphere*, *9*(4), 138.

AghaKouchak, A., F. Chiang, L. S. Huning, C. A. Love, I. Mallakpour, O. Mazdiyasni, H. Moftakhari, S. M. Papalexiou, E. Ragno, and M. Sadegh (2020), Climate Extremes and Compound Hazards in a Warming World, *Annual Review of Earth and Planetary Sciences*, *48*(1), 519–548, doi:10.1146/annurev-earth-071719-055228.

Almazroui, M., M. N. Islam, F. Saeed, S. Saeed, M. Ismail, M. A. Ehsan, I. Diallo, E. O'Brien, M. Ashfaq, D. Martínez-Castro, et al. (2021), Projected changes in temperature and precipitation over the united states, central america, and the caribbean in cmip6 gcms, *Earth Systems and Environment*, *5*, 1–24.

Beaudin, É., E. Di Lorenzo, A. Miller, H. Seo, and Y. Joh (2023), Impact of Extratropical Northeast Pacific SST on US West Coast Precipitation, *Geophysical Research Letters*, *50*(3), e2022GL102,354.

Bhattacharya, T. (2022), An Energetic Perspective on the Holocene North American Monsoon, *Geophysical Research Letters*, *49*(19), e2022GL100,782.

Bhattacharya, Tripti and Feng, Ran and Tierney, Jessica E and Rubbelke, Claire and Burls, Natalie and Knapp, Scott and Fu, Minmin (2022), Expansion and intensification of the north american monsoon during the pliocene, *AGU Advances*, *3*(6), e2022AV000,757.

Bieda, S. W., C. L. Castro, S. L. Mullen, A. C. Comrie, and E. Pytlak (2009), The relationship of transient upper-level troughs to variability of the North American monsoon system, *Journal of Climate*, *22*(15), 4213–4227.

Bordoni, S., and B. Stevens (2006), Principal component analysis of the summertime winds over the Gulf of California: A gulf surge index, *Monthly weather review*, *134*(11), 3395–3414.

Canon, G. (2022), Record death valley flooding 'a once-in-1,000-year event', *The Guardian*.

Capotondi, A., M. Newman, T. Xu, and E. Di Lorenzo (2022), An optimal precursor of Northeast Pacific marine heatwaves and Central Pacific El Niño events, *Geophysical Research Letters*, *49*(5), e2021GL097,350.

Carrillo, C. M., C. L. Castro, C. A. Woodhouse, and D. Griffin (2016), Low-frequency variability of precipitation in the North American monsoon region as diagnosed through earlywood and latewood tree-ring chronologies in the southwestern US, *International Journal of Climatology*, *36*(5), 2254–2272.

Castro, C. L., T. B. McKee, and R. A. Pielke (2001), The relationship of the North American monsoon to tropical and North Pacific sea surface temperatures as revealed by observational analyses, *Journal of Climate*, *14*(24), 4449–4473.

Castro, C. L., R. A. Pielke, J. O. Adegoke, S. D. Schubert, and P. J. Pegion (2007), Investigation of the summer climate of the contiguous United States and Mexico using the Regional Atmospheric Modeling System (RAMS). Part II: Model climate variability, *Journal of Climate*, *20*(15), 3866–3887.

Cavazos, T., C. Turrent, and D. Lettenmaier (2008), Extreme precipitation trends associated with tropical cyclones in the core of the North American monsoon, *Geophysical Research Letters*, *35*(21).

Chang, P., S. Zhang, G. Danabasoglu, S. G. Yeager, H. Fu, H. Wang, F. S. Castruccio, Y. Chen, J. Edwards, D. Fu, et al. (2020), An unprecedented set of high-resolution earth system simulations for understanding multiscale interactions in climate variability and change, *Journal of Advances in Modeling Earth Systems*, *12*(12), e2020MS002,298.

Cook, B. I., and R. Seager (2013), The response of the North American Monsoon to increased greenhouse gas forcing, *Journal of Geophysical Research: Atmospheres*, *118*(4), 1690–1699.

Demaria, E. M., P. Hazenberg, R. L. Scott, M. B. Meles, M. Nichols, and D. Goodrich (2019), Intensification of the North American Monsoon rainfall as observed from a long-term high-density gauge network, *Geophysical Research Letters*, *46*(12), 6839–6847.

Di Lorenzo, E., T. Xu, Y. Zhao, M. Newman, A. Capotondi, S. Stevenson, D. Amaya, B. Anderson, R. Ding, J. Furtado, et al. (2023), Modes and mechanisms of pacific decadal-scale variability, *Annual Review of Marine Science*, *15*, 249–275.

Eyring, V., S. Bony, G. A. Meehl, C. A. Senior, B. Stevens, R. J. Stouffer, and K. E. Taylor (2016), Overview of the coupled model intercomparison project phase 6 (cmip6) experimental design and organization, *Geoscientific Model Development*, *9*(5), 1937–1958.

Fewings, M. R., and K. S. Brown (2019), Regional structure in the marine heat wave of summer 2015 off the western United States, *Frontiers in Marine Science*, *6*, 564.

Fonseca-Hernandez, M., C. Turrent, Y. G. Mayor, and I. Tereshchenko (2021), Using observational and reanalysis data to explore the southern Gulf of California boundary layer during the North American Monsoon onset, *Journal of Geophysical Research: Atmospheres*, *126*(7), e2020JD033,508.

Fu, Minmin and Cane, Mark A and Molnar, Peter and Tziperman, Eli (2022), Warmer pliocene upwelling site sst leads to wetter subtropical coastal areas: A positive feedback on sst, *Paleoceanography and Paleoclimatology*, *37*(2), e2021PA004,357.

Fuller, R. D., and D. J. Stensrud (2000), The relationship between tropical easterly waves and surges over the Gulf of California during the North American monsoon, *Monthly weather review*, *128*(8), 2983–2989.

Griffin, D., C. A. Woodhouse, D. M. Meko, D. W. Stahle, H. L. Faulstich, C. Carrillo, R. Touchan, C. L. Castro, and S. W. Leavitt (2013), North american monsoon precipitation reconstructed from tree-ring latewood, *Geophysical Research Letters*, *40*(5), 954–958.

Haarsma, R. J., M. J. Roberts, P. L. Vidale, C. A. Senior, A. Bellucci, Q. Bao, P. Chang, S. Corti, N. S. Fučkar, V. Guemas, et al. (2016), High resolution model intercomparison project (HighResMIP v1. 0) for CMIP6, *Geoscientific Model Development*, *9*(11), 4185–4208.

Higgins, R., and W. Shi (2005), Relationships between Gulf of California moisture surges and tropical cyclones in the eastern Pacific basin, *Journal of Climate*, *18*(22), 4601–4620.

Higgins, R., W. Shi, and C. Hain (2004), Relationships between Gulf of California moisture surges and precipitation in the southwestern United States, *Journal of Climate*, *17*(15), 2983–2997.

Huang, B., V. F. Banzon, E. Freeman, J. Lawrimore, W. Liu, T. C. Peterson, T. M. Smith, P. W. Thorne, S. D. Woodruff, and H.-M. Zhang (2015), Extended reconstructed sea surface temperature version 4 (ersst. v4). part i: Upgrades and intercomparisons, *Journal of climate*, *28*(3), 911–930.

Ishii, M., A. Shouji, S. Sugimoto, and T. Matsumoto (2005), Objective analyses of sea-surface temperature and marine meteorological variables for the 20th century using icoads and the kobe collection, *International Journal of Climatology: A Journal of the Royal Meteorological Society*, *25*(7), 865–879.

Kalnay, E., M. Kanamitsu, R. Kistler, W. Collins, D. Deaven, L. Gandin, M. Iredell, S. Saha, G. White, J. Woollen, Y. Zhu, M. E. Chelliah, W. Higgins, J. Janowiak, K. Mo, C. Ropelewski, J. Wang, A. Leetmaa, R. Reynolds, R. Jenne, and D. Joseph (1996), The NCEP/NCAR 40-year reanalysis project, *Bulletin of the American meteorological Society*, *77*(3), 437–472.

Kim, H.-M., P. J. Webster, and J. A. Curry (2011), Modulation of North Pacific tropical cyclone activity by three phases of ENSO, *Journal of Climate*, *24*(6), 1839–1849.

Liebmann, B., and C. A. Smith (1996), Description of a complete (interpolated) outgoing longwave radiation dataset, *Bulletin of the American Meteorological Society*, *77*(6), 1275–1277.

Marvel, K., B. I. Cook, C. J. Bonfils, P. J. Durack, J. E. Smerdon, and A. P. Williams (2019), Twentieth-century hydroclimate changes consistent with human influence, *Nature*, *569*(7754), 59–65.

Mauritsen, T., J. Bader, T. Becker, J. Behrens, M. Bittner, R. Brokopf, V. Brovkin, M. Claussen, T. Crueger, M. Esch, I. Fast, S. Fiedler, D. Fläschner, V. Gayler, M. Giorgetta, D. S. Goll, H. Haak, S. Hagemann, C. Hedemann, C. Hohenegger, T. Ilyina, T. Jahns, D. Jimenéz-de-la-Cuesta, J. Jungclaus, T. Kleinen, S. Kloster, D. Kracher, S. Kinne, D. Kleberg, G. Lasslop, L. Kornblueh, J. Marotzke, D. Matei, K. Meraner, U. Mikolajewicz, K. Modali, B. Möbis, W. A. Müller, J. E. M. S. Nabel, C. C. W. Nam, D. Notz, S. Nyawira, H. Paulsen, K. Peters, R. Pincus, H. Pohlmann, J. Pongratz, M. Popp, T. J. Raddatz, S. Rast, R. Redler, C. H. Reick, T. Rohrschneider, V. Schemann, H. Schmidt, R. Schnur, U. Schulzweida, K. D. Six, L. Stein, I. Stemmler, B. Stevens, J. Storch, F. Tian, A. Voigt, P. Vrese, K. Wieners, S. Wilkenskjeld, A. Winkler, and E. Roeckner (2019), Developments in the MPI-M Earth System Model version 1.2 (MPI-ESM1.2) and Its Response to Increasing CO_2, *Journal of Advances in Modeling Earth Systems*, *11*(4), 998–1038, doi:10.1029/2018MS001400.

May, R. M., K. H. Goebbert, J. E. Thielen, J. R. Leeman, M. D. Camron, Z. Bruick, E. C. Bruning, R. P. Manser, S. C. Arms, and P. T. Marsh (2022), MetPy: A meteorological Python library for data analysis and visualization, *Bulletin of the American Meteorological Society*, *103*(10), E2273–E2284.

Mazon, J. J., C. L. Castro, D. K. Adams, H.-I. Chang, C. M. Carrillo, and J. J. Brost (2016), Objective climatological analysis of extreme weather events in Arizona during the North American monsoon, *Journal of Applied Meteorology and Climatology*, *55*(11), 2431–2450.

Mesinger, F., G. DiMego, E. Kalnay, K. Mitchell, P. C. Shafran, W. Ebisuzaki, D. Jović, J. Woollen, E. Rogers, E. H. Berbery, M. B. Ek, Y. Fan, R. Grumbine, W. Higgins, H. Li, Y. Lin, G. Manikin, D. Parrish, and W. Shi (2006), North American regional reanalysis, *Bulletin of the American Meteorological Society*, *87*(3), 343–360.

Meyer, J. D., and J. Jin (2017), The response of future projections of the North American monsoon when combining dynamical downscaling and bias correction of CCSM4 output, *Climate Dynamics*, *49*(1-2), 433–447.

Moloney, K. A., E. L. Mudrak, A. Fuentes-Ramirez, H. Parag, M. Schat, and C. Holzapfel (2019), Increased fire risk in Mojave and Sonoran shrublands due to exotic species and extreme rainfall events, *Ecosphere*, *10*(2), e02,592.

Moon, S., and K.-J. Ha (2020), Future changes in monsoon duration and precipitation using CMIP6, *npj Climate and Atmospheric Science*, *3*(1), 45.

Myers, T. A., C. R. Mechoso, G. V. Cesana, M. J. DeFlorio, and D. E. Waliser (2018), Cloud feedback key to marine heatwave off Baja California, *Geophysical Research Letters*, *45*(9), 4345–4352.

Müller, W. A., J. H. Jungclaus, T. Mauritsen, J. Baehr, M. Bittner, R. Budich, F. Bunzel, M. Esch, R. Ghosh, H. Haak, T. Ilyina, T. Kleine, L. Kornblueh, H. Li, K. Modali, D. Notz, H. Pohlmann, E. Roeckner, I. Stemmler, F. Tian, and J. Marotzke (2018), A Higher-resolution Version of the Max Planck Institute Earth System Model (MPI-ESM1.2-HR), *Journal of Advances in Modeling Earth Systems*, *10*(7), 1383–1413, doi:10.1029/2017MS001217.

O'Mara, N. A., A. H. Cheung, C. S. Kelly, S. Sandwick, T. D. Herbert, J. M. Russell, J. Abella-Gutiérrez, S. G. Dee, P. W. Swarzenski, and J. C. Herguera (2019), Subtropical Pacific Ocean Temperature Fluctuations in the Common Era: Multidecadal Variability and Its Relationship With Southwestern North American Megadroughts, *Geophysical Research Letters*, *46*(24), 14,662–14,673, doi:10.1029/2019GL084828.

Oolman, L. (2006), Wyoming weather web, *University of Wyoming, College of Engineering.[Internet WWW]*.http://weather.uwyo.edu/upperair/bufrraob.shtml.

O'Gorman, P. A. (2015), Precipitation Extremes Under Climate Change, *Current Climate Change Reports*, *1*(2), 49–59, doi:10.1007/s40641-015-0009-3.

Pascale, S., and S. Bordoni (2016), Tropical and extratropical controls of Gulf of California surges and summertime precipitation over the southwestern United States, *Monthly Weather Review*, *144*(7), 2695–2718.

Pascale, S., S. Bordoni, S. B. Kapnick, G. A. Vecchi, L. Jia, T. L. Delworth, S. Underwood, and W. Anderson (2016), The impact of horizontal resolution on north american monsoon gulf of california moisture surges in a suite of coupled global climate models, *Journal of Climate*, *29*(21), 7911–7936.

Pascale, S., W. R. Boos, S. Bordoni, T. L. Delworth, S. B. Kapnick, H. Murakami, G. A. Vecchi, and W. Zhang (2017), Weakening of the North American monsoon with global warming, *Nature Climate Change*, *7*(11), 806–812.

Pascale, S., S. B. Kapnick, S. Bordoni, and T. L. Delworth (2018), The influence of CO2 forcing on North American monsoon moisture surges, *Journal of Climate*, *31*(19), 7949–7968.

Pascale, S., L. M. V. Carvalho, D. K. Adams, C. L. Castro, and I. F. A. Cavalcanti (2019), Current and Future Variations of the Monsoons of the Americas in a Warming Climate, *Current Climate Change Reports*, *5*(3), 125–144, doi:10.1007/s40641-019-00135-w.

Plecha, S. M., and P. M. Soares (2020), Global marine heatwave events using the new CMIP6 multi-model ensemble: from shortcomings in present climate to future projections, *Environmental Research Letters*, *15*(12), 124,058.

Raymond, D. J., C. S. Bretherton, and J. Molinari (2006), Dynamics of the intertropical convergence zone of the east Pacific, *Journal of the atmospheric sciences*, *63*(2), 582–597.

Schneider, U., T. Fuchs, A. Meyer-Christoffer, and B. Rudolf (2008), Global precipitation analysis products of the GPCC, *Global Precipitation Climatology Centre (GPCC), DWD, Internet Publikation*, *112*.

Sillmann, J., V. Kharin, X. Zhang, F. Zwiers, and D. Bronaugh (2013), Climate extremes indices in the CMIP5 multimodel ensemble: Part 1. Model evaluation in the present climate, *Journal of geophysical research: atmospheres*, *118*(4), 1716–1733.

Stensrud, D. J., R. L. Gall, and M. K. Nordquist (1997), Surges over the Gulf of California during the Mexican monsoon, *Monthly Weather Review*, *125*(4), 417–437.

Swain, D. L., M. Tsiang, M. Haugen, D. Singh, A. Charland, B. Rajaratnam, and N. S. Diffenbaugh (2014), The extraordinary California drought of 2013/2014: Character, context, and the role of climate change, *Bulletin of the American Meteorological Society*, *95*(9), S3.

Varuolo-Clarke, A. M., K. A. Reed, and B. Medeiros (2019), Characterizing the North American monsoon in the Community Atmosphere Model: Sensitivity to resolution and topography, *Journal of Climate*, *32*(23), 8355–8372.

Wei, X., K.-Y. Li, T. Kilpatrick, M. Wang, and S.-P. Xie (2021), Large-scale conditions for the record-setting Southern California marine heatwave of August 2018, *Geophysical Research Letters*, *48*(7), e2020GL091,803.

Wilks, D. S. (2011), *Statistical Methods in the Atmospheric Sciences*, vol. 100, Academic press.

Wills, R. C., Y. Dong, C. Proistosecu, K. C. Armour, and D. S. Battisti (2022), Systematic Climate Model Biases in the Large-Scale Patterns of Recent Sea-Surface Temperature and Sea-Level Pressure Change, *Geophysical Research Letters*, *49*(17), e2022GL100,011.

Xie, P., P. A. Arkin, and J. E. Janowiak (2007), CMAP: The CPC merged analysis of precipitation, *Measuring precipitation from space*, *28*, 319–328.

Yang, L., J. Smith, M. L. Baeck, E. Morin, and D. C. Goodrich (2017), Flash flooding in arid/semiarid regions: Dissecting the hydrometeorology and hydrology of the 19 August 2014 storm and flood hydroclimatology in Arizona, *Journal of Hydrometeorology*, *18*(12), 3103–3123.

Zhang, Q., B. Liu, S. Li, and T. Zhou (2023), Understanding Models' Global Sea Surface Temperature Bias in Mean State: From CMIP5 to CMIP6, *Geophysical Research Letters*, *50*(4), doi:10.1029/2022GL100888.

Supplemental Information for *California Margin temperatures modulate extreme summer precipitation in the desert Southwest*

Tripti Bhattacharya[1], Ran Feng[2], Christopher R. Maupin[3], Sloan Coats[4], Peter R. Brennan[1], and Elizabeth Carter[5]

[1]Department of Earth and Environmental Sciences, Syracuse University, Syracuse, NY, USA

[2]Department of Geosciences, University of Connecticut, Storrs, CT, USA

[3]Department of Geography, Texas A&M University, College Station, TX, USA

[4]Department of Earth Sciences, University of Hawai'i at Manoa, Honolulu, HI, USA

[5]Civil and Environmental Engineering, Syracuse University, Syracuse, NY USA

September 20, 2023

Contents of this file

1. Text S1

2. Figures S1 to S9

3. Table S1

Text S1. Additional Methods Description

Correlation and Running Correlation Analysis

To identify the link between CA margin SSTs and monthly mean precipitation over the northern NAM domain, we calculated an index of SSTs between 25 and 32 °N and 125 and 110 °W. We then calculated the linear correlation of this index and monthly mean precipitation fields from the 0.25 °Global Precipitation Climatology Centre (GPCC) product between 1960 and 2014, the Climate Prediction Center merged analysis of precipitation (CPC), the Global Precipitation Climatology Project (GPCP), and the NARR (*Schneider et al.*, 2008; *Xie et al.*, 2007; *Adler et al.*, 2018; *Mesinger et al.*, 2006). Using multiple precipitation products helps establish the robustness of the relationship. We also evaluated the correlation between this SST index and monthly mean fields of SLP, precipitable water, and moisture flux from the NARR.

For our analysis of correlations between CA margin SSTs and precipitation across a range of Coupled Model Intercomparison Project (CMIP) phase 5 and 6 ESMs, we use an index of precipitation over land areas between 27 and 37 °N and 115 and 107 °W. For the SST-sea level pressure (SLP) correlation analysis, we use an index of SLP over ocean areas between 20 and 30 °N and 125 and 110 °W. Slight changes to the bounds of these index regions do not alter our results or conclusions.

In Figure **S13**, we plot the running correlation between CA margin SST anomalies and precipitation in future emission scenarios for the 4 ESMs that show the greatest fidelity over the historical period at producing the observed SST-precipitation correlation (high resolution configurations of CESM1.3, MPI-ESM1-2, as well as ACCESS-CM and CanESM5). This running correlation is performed in 40-year averaging windows for historical simulations, Shared Socioeconomic Pathway (SSP) 3-7.0 and 5-8.5 in the case of the MPI, ACCESS and CanESM5 ESMs, and for Representative Concentration Pathway (RCP) 8.5 in the case of CESM1.3-HR (see Table S1 for more details). Because the forcing datasets differ across these simulations, the purpose of this analysis is not to analyze the particular trajectory of NAM precipitation and SST in a given ESM versus another, although we show this in Figure **S12**. Instead, the goal of this analysis is show that the strength of the correlation between CA margin SSTs and northern NAM precipitation remains statistically significant in the future.

Contrasting Models with High and Low Skill

Figure 4 in the main text contrasts models with high and low skill at reproducing the SST-monsoon linkage (e.g. the correlation between CA margin SSTs averaged between 25 and 32 °N and 125 and 110 °W and NAM precipitation). To create composite correlation plots contrasting the best and worst models, each models' fields of 850 mb geopotential height, sea level pressure, zonal and meridional moisture flux (calculated from inputs of u and v winds as well as humidity), and precipitation from historical simulations were regridded to a common 1 °by 1 °latitude and longitude grid. We used these regridded model fields to calculate the correlation between the timeseries of each models' CA margin SST index and that models' timeseries of geopotential height, sea level pressure, moisture flux, and precipitation. Correlation fields from the good models (e.g. CESM1.3; MPI-ESM-1-2-HR; ACCESS-CM2; CanESM5-1) are averaged together to generate a 'composite' correlation field representing the good models. Similarly, climatologies of each variable from each model are computed and then averaged together to create a composite climatology for these 'good models.' These results are presented in Figure 4 in the main text and Figure S7. The same procedure is repeated for the worst performing models (e.g. NESM3; FIO-ESM2; MIROC6) to create a composite of worst-performing models.

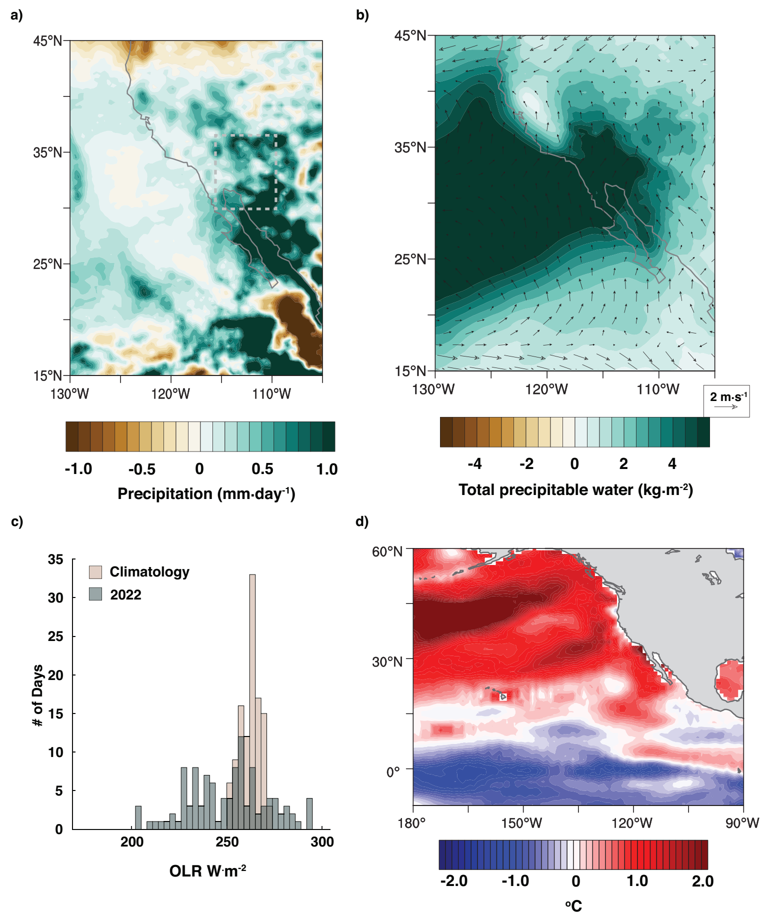

Figure S1: **Shifts in monsoon precipitation rates in summer 2022.** a) shows July-September monthly mean precipitation anomalies in mm/day. Gray box highlights the northern NAM region used for averaging, and includes Death Valley, CA. b) shows anomalies of total precipitable water and 850 mb winds. c) shows differences in daily values of outgoing longwave radiation (OLR) for summer 2022 (mint green) compared to the climatology between 1974 and 2022 (tan). The distribution of OLR for 2022 is significantly different from the climatological distribution at the 95% level according to a 2-sided Kolmogorov-Smirnov (K-S) test. d) shows summer 2022 SST anomalies in °C relative to a 1950-2022 climatology.

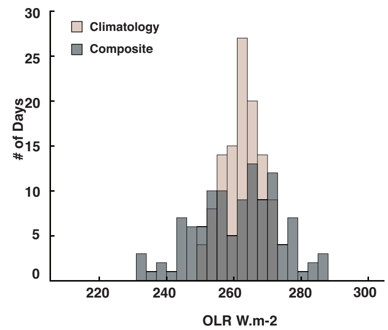

Figure S2: Differences in daily values of outgoing longwave radiation (OLR) for five summers with the greatest extreme precipitation days (mint green) compared to the climatology between 1974 and 2022 (tan). The distribution of OLR for extreme precipitation years is significantly different from the climatological distribution at the 95% level according to a 2-sided Kolmogorov-Smirnov (K-S) test.

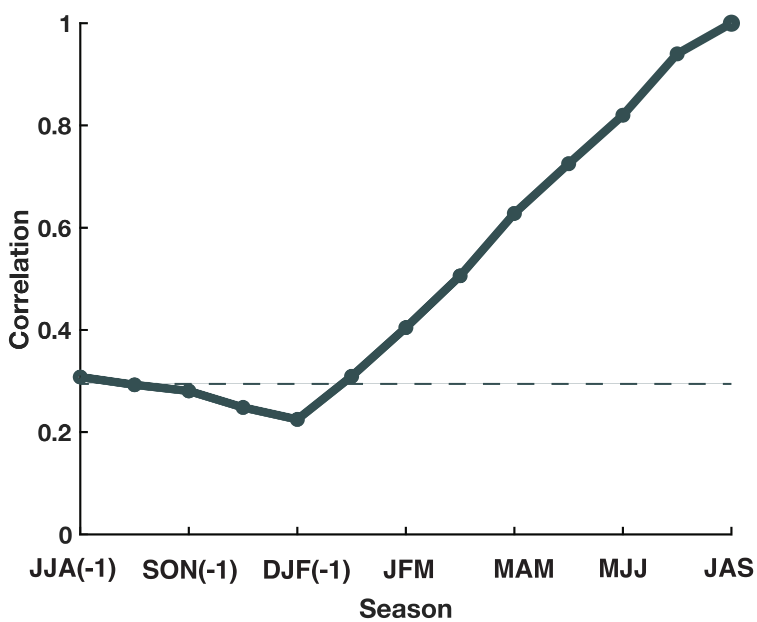

Figure S3: Correlation between July-September (JAS) SST anomalies on the CA Margin (25 and 32 °N and 125 and 110 °W) and simultaneous (JAS) and prior seasons' SST anomalies, starting with JJA, then MJJ, AMJ, MAM, etc. until JJA in the prior year. Significance of correlation level is indicated by the dashed line.

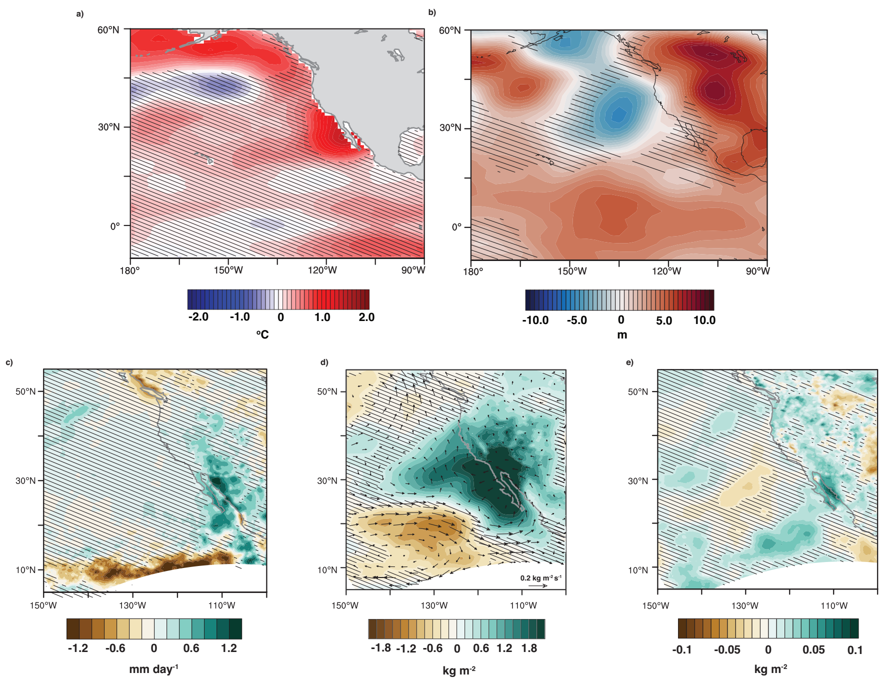

Figure S4: Fields shown in Figure 1 in main text, with shading to indicate regions where composite anomalies are not statistically significant. a) SST; b) 850 mb geopotential height; c) NARR monthly mean precipitation rate d) moisture flux and total precipitable water (shading indicates significance of precipitable water composite anomalies). e) evaporation. Significance determined via a two-sided t-test.

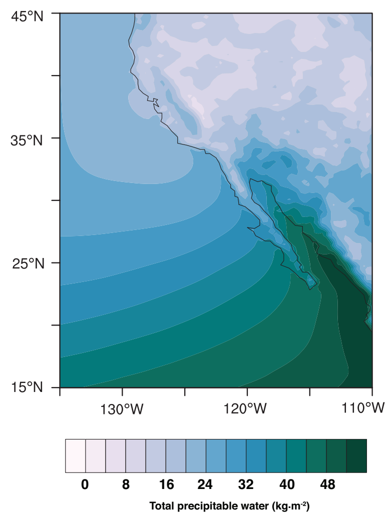

Figure S5: July-September climatology of total precipitable water in kg/m^2 over the southwest US and western Mexico. Data from the North American Regional Reanalysis (*Mesinger et al.*, 2006). Climatology shows strong gradients from 30-40 °N, where there are very low values of precipitable water over desert regions of the southwest.

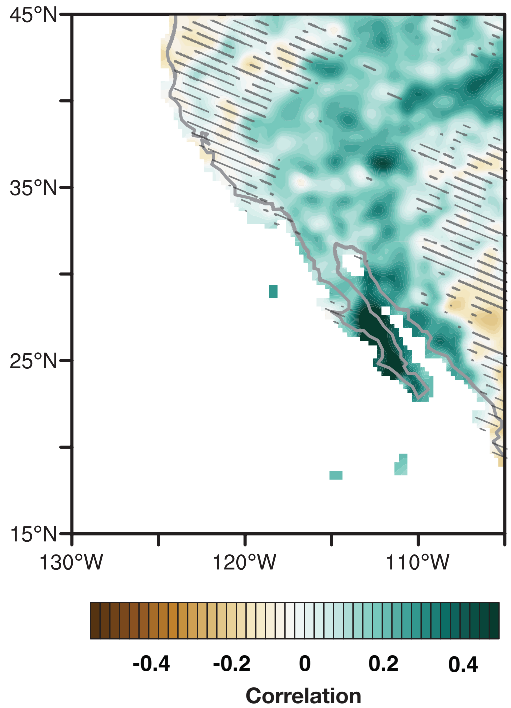

Figure S6: Correlation between CA Margin SSTs and GPCC precipitation in GPCC precipitation. SSTs are an index between 25 and 32 °N and 125 and 110 °W, taken from the COBE SST product (*Ishii et al.*, 2005). Shading indicates regions where correlation is not statistically significant. See next figure for correlation with multiple products

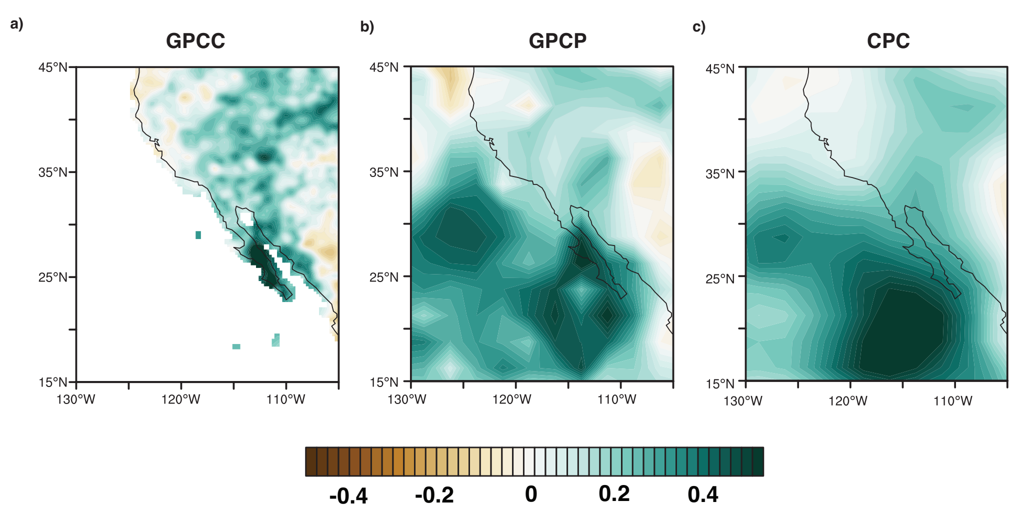

Figure S7: Correlation between CA Margin SSTs and precipitation in multiple products. SSTs are an index between 25 and 32 °N and 125 and 110 °W, taken from the COBE SST product (*Ishii et al.*, 2005).

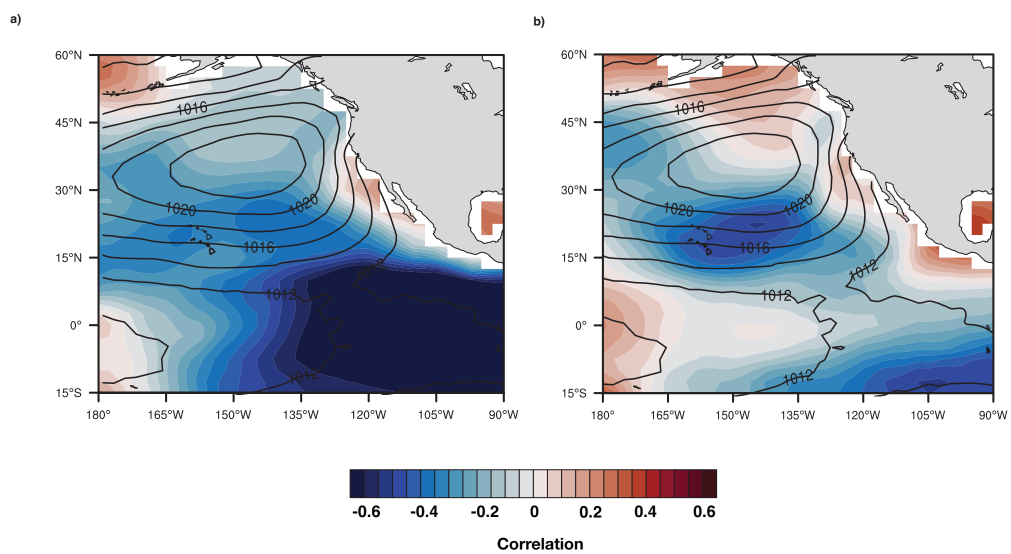

Figure S8: Correlation between sea level pressure (SLP) over the northeast Pacific and other modes of variability. a) shows simultaneous correlation between Niño 3.4 index and SLP; b) shows simultaneous correlation between the Pacific Decadal Oscillation (PDO) and SLP. Solid contours represent climatological values of SLP

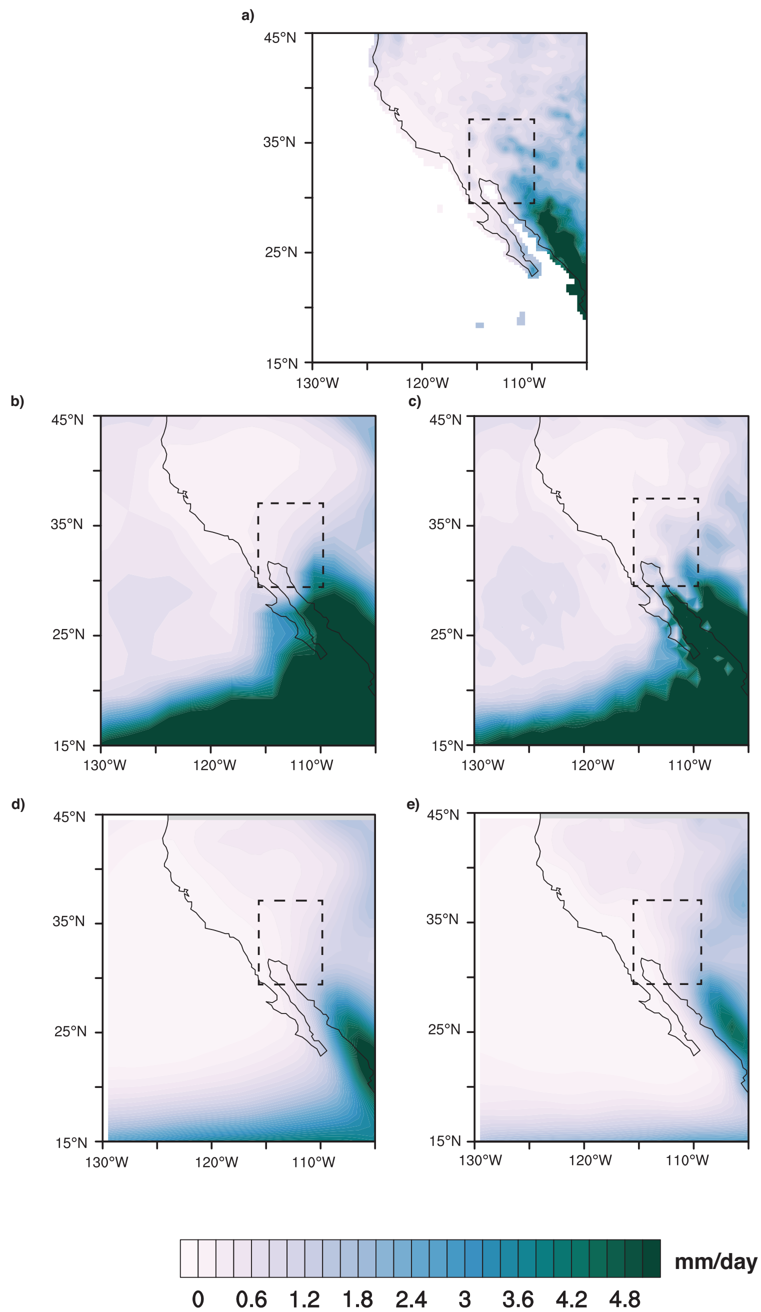

Figure S9: July-September climatology of low vs. high resolution ESMs. a) shows observational climatology of summertime precipitation from the GPCC 0.25 °product; b) shows MPI-ESM1-2 low resolution summertime rainfall climatology; c) shows MPI-ESM1-2 high resolution climatology; d) shows CESM1.3 low resolution climatology; e) shows CESM1.3 high resolution climatology. All ESM climatologies are computed from 1950-2014 in historical simulations. Dashed box outlines the region used for precipitation averages shown in Figure 5 in the main text. Climatologies of rainfall rates show only a small improvement over this dashed box in the high resolution version of the ESMs

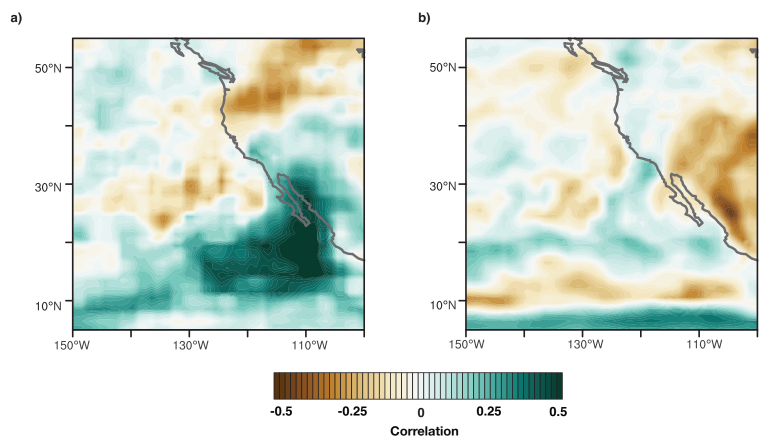

Figure S10: July-September correlation of precipitation with CA margin SST anomalies (see text for index definition) contrasting models that perform well and those that perform poorly. a) shows models with good skill at reproducing SST-monsoon linkage (CESM1.3; ACCESS-CM2; CanESM5-1; MPI-ESM-1-2-HR) and b) shows model with poor skill at simulating linkage (FIO-ESM-2; NESM3; MIROC6).

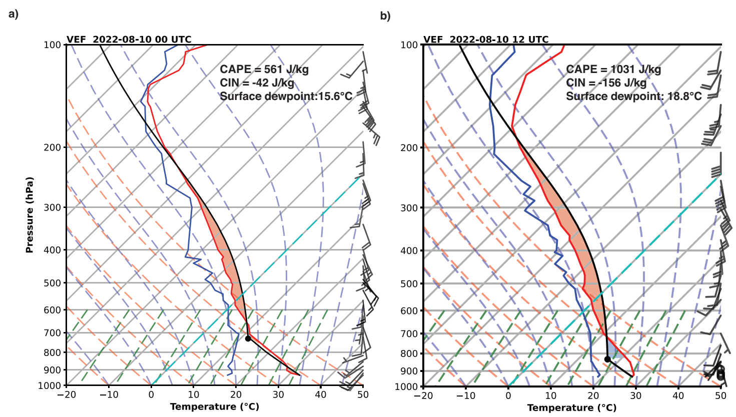

Figure S11: Las Vegas (VEF) observed soundings, 10 August 2022 at a) 00Z and b) 12Z. Atmospheric temperature (red), dewpoint temperature (blue) and windspeed with direction (barbs) shown as a function of atmospheric pressure. Profiles (black line) are calculated by dry adiabatic lifting of parcels to the lifted condensation level (LCL, filled black circle). Convective inhibition (CIN; blue shading) and convective available potential energy (CAPE; red shading) are calculated from the surface to the LCL, and from the surface to the equilibrium level (EL), respectively. Both soundings document nearly identical precipitable water amounts, despite a nearly twofold jump in CAPE within 12 hours. The increase in instability is associated with a turning of the low-level winds from southwesterly to southerly. A corresponding moistening from the surface to 700 hPa from this southerly transport, visible when comparing sounding dewpoint temperatures, lowers the LCL, contributing to the strong increase in instability and CAPE.

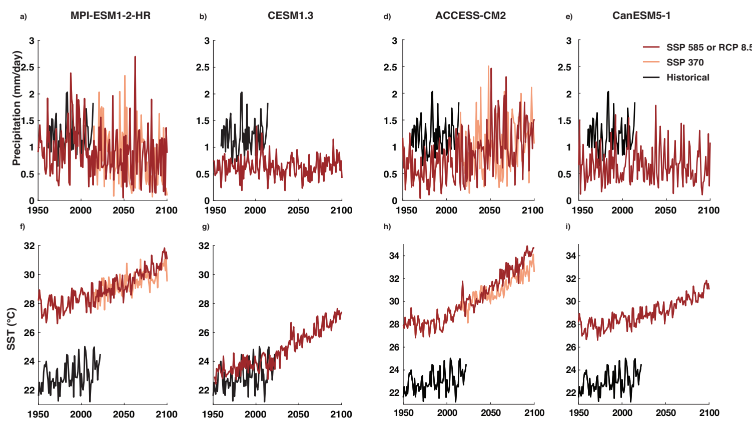

Figure S12: 21st century changes in precipitation and SST for ESMs that exhibit CA margin SST-northern NAM rainfall correlations similar to observations. Top panel shows precipitation (mm/day); bottom panel shows SST (°C). a) and f) are MPI-ESM1-2; b) and g) are CESM1.3; c) and h) are ACCESS-CM2; and d) and i) are CanESM5-1. SSTs and precipitation are in absolute units rather than anomalies in order to highlight SST and precipitation biases.

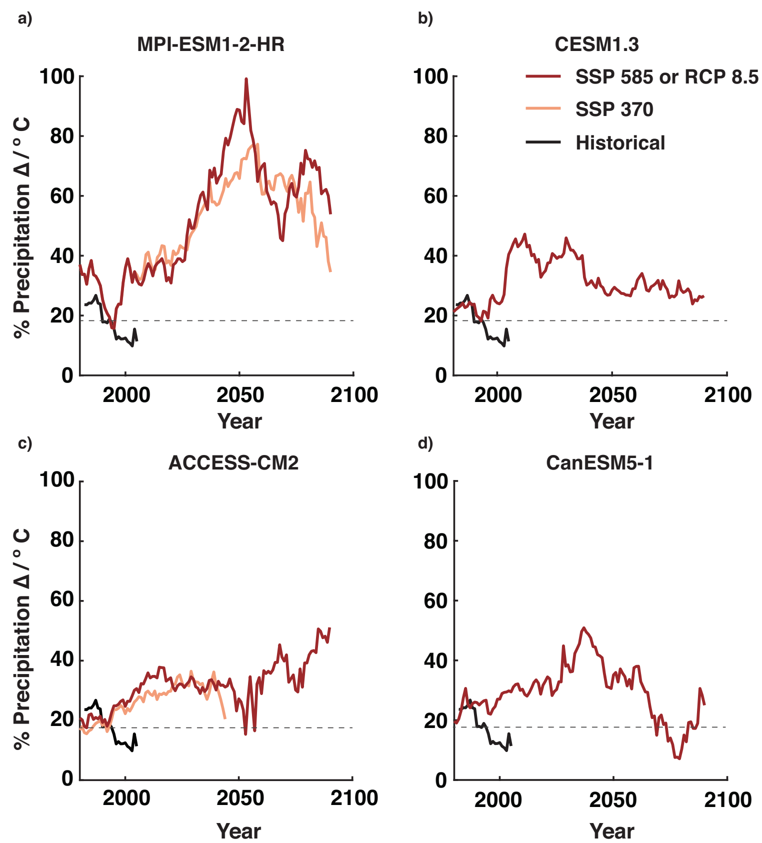

Figure S13: Running correlation between CA margin SST and precipitation for future emissions scenarios across four ESMs that show the highest skill at reproducing the observed SST-precipitation correlation (see Figure 4 in main text). Correlations above the dashed line are statistically significant at the 95% level.

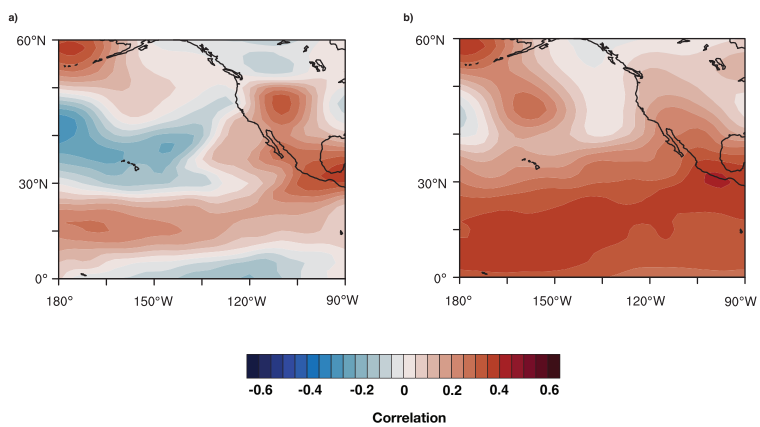

Figure S14: Contrasting correlation patterns between geopotential height and CA margin SST index in NCEP-NCAR reanalysis. a) shows 850 mb heights (similar to the pattern in Figure 2 in the main text); b) shows 500 mb height pattern.

Table S1: CMIP6 and CMIP5 models used to analyze the relationship between SST bias between 22 and 30 °N and 125 and 110 °W, on the CA margin, and the relationship between SSTs, precipitation, and SLP over northern NAM domain shown in Figure 4 and Figure 5 in the main text. Acronym refers to the acronym used in Figure 4 in the main text.

Institution	Model Name	Acronym	Simulations Analyzed
National Center for Atmospheric Research	CESM2	CESM2	CMIP6 historical
National Center for Atmospheric Research	CESM1.3 low-res	CESM1.3 LR	CMIP5 historical
National Center for Atmospheric Research	CESM1.3 high-res	CESM1.3 HR	CMIP5 historical RCP8.5
EC Earth Consortium	EC-Earth3	ECEarth3	CMIP6 historical
Model for Interdisciplinary Research on Climate	MIROC6	MIROC6	CMIP6 historical
Model for Interdisciplinary Research on Climate	MIROC-ESM2-L	MIROC-ESML	CMIP6 historical
Geophysical Fluid Dynamics Laboratory	GFDL-CM4	GFDL-CM4	CMIP6 historical
Geophysical Fluid Dynamics Laboratory	GFDL-ESM4	GFDL-ESM4	CMIP6 historical
L'Institut Pierre-Simon Laplace	IPSL-CM6A-LR	IPSL-CM6A-LR	CMIP6 historical
Beijing Climate Center	BCC-CSM2-MR	BCC	CMIP6 historical
State Key Laboratory of Numerical Modeling for Atmospheric Sciences and Geophysical Fluid Dynamics	FGOALS-g3	FGOALS	CMIP6 historical
Max Planck Institute for Meteorology	MPI-ESM1-2-LR	MPI-LR	CMIP6 historical
Max Planck Institute for Meteorology	MPI-ESM1-2-HR	MPI-HR	CMIP6 historical SSP585 SSP370
Canadian Centre for Climate Modelling and Analysis	CanESM5-1	CanESM5	CMIP6 historical SSP585
Centre National de Recherches Météorologiques	CNRM-CM6-1	CNRM-LR	CMIP6 historical
Centre National de Recherches Météorologiques	CNRM-CM6-1	CNRM-HR	CMIP6 historical
Commonwealth Scientific & Industrial Research Organisation Australia	ACCESS-CM2	ACCESS-CM	CMIP6 historical SSP585 SSP370
Commonwealth Scientific and Industrial Research Organisation Australia	ACCESS-ESM2	ACCESS-ESM	CMIP6 historical
Nanjing University of Information Science and Technology China	NESM3	NESM3	CMIP6 historical
First Institute of Oceanography and Pilot National Laboratory for Marine Science and Technology	FIO-ESM2	IO-ESM2	CMIP6 historical
Meteorological Research Institute Japan	MRI-ESM-2.0	MRI-ESM2	CMIP6 historical
Institute for Numerical Mathematics Russian Federation	INM-CM4-8	INM4-8	CMIP6 historical
Institute for Numerical Mathematics Russian Federation	INM-CM5-0	INM5-0	CMIP6 historical

References

Adams, D. K., and A. C. Comrie (1997), The north american monsoon, *Bulletin of the American Meteorological Society*, *78*(10), 2197–2214.

Adams, J. L., and D. J. Stensrud (2007), Impact of tropical easterly waves on the North American monsoon, *Journal of climate*, *20*(7), 1219–1238.

Adler, R. F., M. R. Sapiano, G. J. Huffman, J.-J. Wang, G. Gu, D. Bolvin, L. Chiu, U. Schneider, A. Becker, E. Nelkin, P. Xie, R. Ferraro, and D.-B. Shin (2018), The global precipitation climatology project (gpcp) monthly analysis (new version 2.3) and a review of 2017 global precipitation, *Atmosphere*, *9*(4), 138.

AghaKouchak, A., F. Chiang, L. S. Huning, C. A. Love, I. Mallakpour, O. Mazdiyasni, H. Moftakhari, S. M. Papalexiou, E. Ragno, and M. Sadegh (2020), Climate Extremes and Compound Hazards in a Warming World, *Annual Review of Earth and Planetary Sciences*, *48*(1), 519–548, doi:10.1146/annurev-earth-071719-055228.

Almazroui, M., M. N. Islam, F. Saeed, S. Saeed, M. Ismail, M. A. Ehsan, I. Diallo, E. O'Brien, M. Ashfaq, D. Martínez-Castro, et al. (2021), Projected changes in temperature and precipitation over the united states, central america, and the caribbean in cmip6 gcms, *Earth Systems and Environment*, *5*, 1–24.

Beaudin, É., E. Di Lorenzo, A. Miller, H. Seo, and Y. Joh (2023), Impact of Extratropical Northeast Pacific SST on US West Coast Precipitation, *Geophysical Research Letters*, *50*(3), e2022GL102,354.

Bhattacharya, T. (2022), An Energetic Perspective on the Holocene North American Monsoon, *Geophysical Research Letters*, *49*(19), e2022GL100,782.

Bhattacharya, Tripti and Feng, Ran and Tierney, Jessica E and Rubbelke, Claire and Burls, Natalie and Knapp, Scott and Fu, Minmin (2022), Expansion and intensification of the north american monsoon during the pliocene, *AGU Advances*, *3*(6), e2022AV000,757.

Bieda, S. W., C. L. Castro, S. L. Mullen, A. C. Comrie, and E. Pytlak (2009), The relationship of transient upper-level troughs to variability of the North American monsoon system, *Journal of Climate*, *22*(15), 4213–4227.

Bordoni, S., and B. Stevens (2006), Principal component analysis of the summertime winds over the Gulf of California: A gulf surge index, *Monthly weather review*, *134*(11), 3395–3414.

Canon, G. (2022), Record death valley flooding 'a once-in-1,000-year event', *The Guardian*.

Capotondi, A., M. Newman, T. Xu, and E. Di Lorenzo (2022), An optimal precursor of Northeast Pacific marine heatwaves and Central Pacific El Niño events, *Geophysical Research Letters*, *49*(5), e2021GL097,350.

Carrillo, C. M., C. L. Castro, C. A. Woodhouse, and D. Griffin (2016), Low-frequency variability of precipitation in the North American monsoon region as diagnosed through earlywood and latewood tree-ring chronologies in the southwestern US, *International Journal of Climatology*, *36*(5), 2254–2272.

Castro, C. L., T. B. McKee, and R. A. Pielke (2001), The relationship of the North American monsoon to tropical and North Pacific sea surface temperatures as revealed by observational analyses, *Journal of Climate*, *14*(24), 4449–4473.

Castro, C. L., R. A. Pielke, J. O. Adegoke, S. D. Schubert, and P. J. Pegion (2007), Investigation of the summer climate of the contiguous United States and Mexico using the Regional Atmospheric Modeling System (RAMS). Part II: Model climate variability, *Journal of Climate*, *20*(15), 3866–3887.

Cavazos, T., C. Turrent, and D. Lettenmaier (2008), Extreme precipitation trends associated with tropical cyclones in the core of the North American monsoon, *Geophysical Research Letters*, *35*(21).

Chang, P., S. Zhang, G. Danabasoglu, S. G. Yeager, H. Fu, H. Wang, F. S. Castruccio, Y. Chen, J. Edwards, D. Fu, et al. (2020), An unprecedented set of high-resolution earth system simulations for understanding multiscale interactions in climate variability and change, *Journal of Advances in Modeling Earth Systems*, *12*(12), e2020MS002,298.

Cook, B. I., and R. Seager (2013), The response of the North American Monsoon to increased greenhouse gas forcing, *Journal of Geophysical Research: Atmospheres*, *118*(4), 1690–1699.

Demaria, E. M., P. Hazenberg, R. L. Scott, M. B. Meles, M. Nichols, and D. Goodrich (2019), Intensification of the North American Monsoon rainfall as observed from a long-term high-density gauge network, *Geophysical Research Letters*, *46*(12), 6839–6847.

Di Lorenzo, E., T. Xu, Y. Zhao, M. Newman, A. Capotondi, S. Stevenson, D. Amaya, B. Anderson, R. Ding, J. Furtado, et al. (2023), Modes and mechanisms of pacific decadal-scale variability, *Annual Review of Marine Science*, *15*, 249–275.

Eyring, V., S. Bony, G. A. Meehl, C. A. Senior, B. Stevens, R. J. Stouffer, and K. E. Taylor (2016), Overview of the coupled model intercomparison project phase 6 (cmip6) experimental design and organization, *Geoscientific Model Development*, *9*(5), 1937–1958.

Fewings, M. R., and K. S. Brown (2019), Regional structure in the marine heat wave of summer 2015 off the western United States, *Frontiers in Marine Science*, *6*, 564.

Fonseca-Hernandez, M., C. Turrent, Y. G. Mayor, and I. Tereshchenko (2021), Using observational and reanalysis data to explore the southern Gulf of California boundary layer during the North American Monsoon onset, *Journal of Geophysical Research: Atmospheres*, *126*(7), e2020JD033,508.

Fu, Minmin and Cane, Mark A and Molnar, Peter and Tziperman, Eli (2022), Warmer pliocene upwelling site sst leads to wetter subtropical coastal areas: A positive feedback on sst, *Paleoceanography and Paleoclimatology*, *37*(2), e2021PA004,357.

Fuller, R. D., and D. J. Stensrud (2000), The relationship between tropical easterly waves and surges over the Gulf of California during the North American monsoon, *Monthly weather review*, *128*(8), 2983–2989.

Griffin, D., C. A. Woodhouse, D. M. Meko, D. W. Stahle, H. L. Faulstich, C. Carrillo, R. Touchan, C. L. Castro, and S. W. Leavitt (2013), North american monsoon precipitation reconstructed from tree-ring latewood, *Geophysical Research Letters*, *40*(5), 954–958.

Haarsma, R. J., M. J. Roberts, P. L. Vidale, C. A. Senior, A. Bellucci, Q. Bao, P. Chang, S. Corti, N. S. Fučkar, V. Guemas, et al. (2016), High resolution model intercomparison project (HighResMIP v1. 0) for CMIP6, *Geoscientific Model Development*, *9*(11), 4185–4208.

Higgins, R., and W. Shi (2005), Relationships between Gulf of California moisture surges and tropical cyclones in the eastern Pacific basin, *Journal of Climate*, *18*(22), 4601–4620.

Higgins, R., W. Shi, and C. Hain (2004), Relationships between Gulf of California moisture surges and precipitation in the southwestern United States, *Journal of Climate*, *17*(15), 2983–2997.

Huang, B., V. F. Banzon, E. Freeman, J. Lawrimore, W. Liu, T. C. Peterson, T. M. Smith, P. W. Thorne, S. D. Woodruff, and H.-M. Zhang (2015), Extended reconstructed sea surface temperature version 4 (ersst. v4). part i: Upgrades and intercomparisons, *Journal of climate*, *28*(3), 911–930.

Ishii, M., A. Shouji, S. Sugimoto, and T. Matsumoto (2005), Objective analyses of sea-surface temperature and marine meteorological variables for the 20th century using icoads and the kobe collection, *International Journal of Climatology: A Journal of the Royal Meteorological Society*, *25*(7), 865–879.

Kalnay, E., M. Kanamitsu, R. Kistler, W. Collins, D. Deaven, L. Gandin, M. Iredell, S. Saha, G. White, J. Woollen, Y. Zhu, M. E. Chelliah, W. Higgins, J. Janowiak, K. Mo, C. Ropelewski, J. Wang, A. Leetmaa, R. Reynolds, R. Jenne, and D. Joseph (1996), The NCEP/NCAR 40-year reanalysis project, *Bulletin of the American meteorological Society*, *77*(3), 437–472.

Kim, H.-M., P. J. Webster, and J. A. Curry (2011), Modulation of North Pacific tropical cyclone activity by three phases of ENSO, *Journal of Climate*, *24*(6), 1839–1849.

Liebmann, B., and C. A. Smith (1996), Description of a complete (interpolated) outgoing longwave radiation dataset, *Bulletin of the American Meteorological Society*, *77*(6), 1275–1277.

Marvel, K., B. I. Cook, C. J. Bonfils, P. J. Durack, J. E. Smerdon, and A. P. Williams (2019), Twentieth-century hydroclimate changes consistent with human influence, *Nature*, *569*(7754), 59–65.

Mauritsen, T., J. Bader, T. Becker, J. Behrens, M. Bittner, R. Brokopf, V. Brovkin, M. Claussen, T. Crueger, M. Esch, I. Fast, S. Fiedler, D. Fläschner, V. Gayler, M. Giorgetta, D. S. Goll, H. Haak, S. Hagemann, C. Hedemann, C. Hohenegger, T. Ilyina, T. Jahns, D. Jimenéz-de-la-Cuesta, J. Jungclaus, T. Kleinen, S. Kloster, D. Kracher, S. Kinne, D. Kleberg, G. Lasslop, L. Kornblueh, J. Marotzke, D. Matei, K. Meraner, U. Mikolajewicz, K. Modali, B. Möbis, W. A. Müller, J. E. M. S. Nabel, C. C. W. Nam, D. Notz, S. Nyawira, H. Paulsen, K. Peters, R. Pincus, H. Pohlmann, J. Pongratz, M. Popp, T. J. Raddatz, S. Rast, R. Redler, C. H. Reick, T. Rohrschneider, V. Schemann, H. Schmidt, R. Schnur, U. Schulzweida, K. D. Six, L. Stein, I. Stemmler, B. Stevens, J. Storch, F. Tian, A. Voigt, P. Vrese, K. Wieners, S. Wilkenskjeld, A. Winkler, and E. Roeckner (2019), Developments in the MPI-M Earth System Model version 1.2 (MPI-ESM1.2) and Its Response to Increasing CO_2, *Journal of Advances in Modeling Earth Systems*, *11*(4), 998–1038, doi:10.1029/2018MS001400.

May, R. M., K. H. Goebbert, J. E. Thielen, J. R. Leeman, M. D. Camron, Z. Bruick, E. C. Bruning, R. P. Manser, S. C. Arms, and P. T. Marsh (2022), MetPy: A meteorological Python library for data analysis and visualization, *Bulletin of the American Meteorological Society*, *103*(10), E2273–E2284.

Mazon, J. J., C. L. Castro, D. K. Adams, H.-I. Chang, C. M. Carrillo, and J. J. Brost (2016), Objective climatological analysis of extreme weather events in Arizona during the North American monsoon, *Journal of Applied Meteorology and Climatology*, *55*(11), 2431–2450.

Mesinger, F., G. DiMego, E. Kalnay, K. Mitchell, P. C. Shafran, W. Ebisuzaki, D. Jović, J. Woollen, E. Rogers, E. H. Berbery, M. B. Ek, Y. Fan, R. Grumbine, W. Higgins, H. Li, Y. Lin, G. Manikin, D. Parrish, and W. Shi (2006), North American regional reanalysis, *Bulletin of the American Meteorological Society*, *87*(3), 343–360.

Meyer, J. D., and J. Jin (2017), The response of future projections of the North American monsoon when combining dynamical downscaling and bias correction of CCSM4 output, *Climate Dynamics*, *49*(1-2), 433–447.

Moloney, K. A., E. L. Mudrak, A. Fuentes-Ramirez, H. Parag, M. Schat, and C. Holzapfel (2019), Increased fire risk in Mojave and Sonoran shrublands due to exotic species and extreme rainfall events, *Ecosphere*, *10*(2), e02,592.

Moon, S., and K.-J. Ha (2020), Future changes in monsoon duration and precipitation using CMIP6, *npj Climate and Atmospheric Science*, *3*(1), 45.

Myers, T. A., C. R. Mechoso, G. V. Cesana, M. J. DeFlorio, and D. E. Waliser (2018), Cloud feedback key to marine heatwave off Baja California, *Geophysical Research Letters*, *45*(9), 4345–4352.

Müller, W. A., J. H. Jungclaus, T. Mauritsen, J. Baehr, M. Bittner, R. Budich, F. Bunzel, M. Esch, R. Ghosh, H. Haak, T. Ilyina, T. Kleine, L. Kornblueh, H. Li, K. Modali, D. Notz, H. Pohlmann, E. Roeckner, I. Stemmler, F. Tian, and J. Marotzke (2018), A Higher-resolution Version of the Max Planck Institute Earth System Model (MPI-ESM1.2-HR), *Journal of Advances in Modeling Earth Systems*, *10*(7), 1383–1413, doi:10.1029/2017MS001217.

O'Mara, N. A., A. H. Cheung, C. S. Kelly, S. Sandwick, T. D. Herbert, J. M. Russell, J. Abella-Gutiérrez, S. G. Dee, P. W. Swarzenski, and J. C. Herguera (2019), Subtropical Pacific Ocean Temperature Fluctuations in the Common Era: Multidecadal Variability and Its Relationship With Southwestern North American Megadroughts, *Geophysical Research Letters*, *46*(24), 14,662–14,673, doi:10.1029/2019GL084828.

Oolman, L. (2006), Wyoming weather web, *University of Wyoming, College of Engineering.[Internet WWW]*.`http://weather.uwyo.edu/upperair/bufrraob.shtml`.

O'Gorman, P. A. (2015), Precipitation Extremes Under Climate Change, *Current Climate Change Reports*, *1*(2), 49–59, doi:10.1007/s40641-015-0009-3.

Pascale, S., and S. Bordoni (2016), Tropical and extratropical controls of Gulf of California surges and summertime precipitation over the southwestern United States, *Monthly Weather Review*, *144*(7), 2695–2718.

Pascale, S., S. Bordoni, S. B. Kapnick, G. A. Vecchi, L. Jia, T. L. Delworth, S. Underwood, and W. Anderson (2016), The impact of horizontal resolution on north american monsoon gulf of california moisture surges in a suite of coupled global climate models, *Journal of Climate*, *29*(21), 7911–7936.

Pascale, S., W. R. Boos, S. Bordoni, T. L. Delworth, S. B. Kapnick, H. Murakami, G. A. Vecchi, and W. Zhang (2017), Weakening of the North American monsoon with global warming, *Nature Climate Change*, *7*(11), 806–812.

Pascale, S., S. B. Kapnick, S. Bordoni, and T. L. Delworth (2018), The influence of CO2 forcing on North American monsoon moisture surges, *Journal of Climate*, *31*(19), 7949–7968.

Pascale, S., L. M. V. Carvalho, D. K. Adams, C. L. Castro, and I. F. A. Cavalcanti (2019), Current and Future Variations of the Monsoons of the Americas in a Warming Climate, *Current Climate Change Reports*, *5*(3), 125–144, doi:10.1007/s40641-019-00135-w.

Plecha, S. M., and P. M. Soares (2020), Global marine heatwave events using the new CMIP6 multi-model ensemble: from shortcomings in present climate to future projections, *Environmental Research Letters*, *15*(12), 124,058.

Raymond, D. J., C. S. Bretherton, and J. Molinari (2006), Dynamics of the intertropical convergence zone of the east Pacific, *Journal of the atmospheric sciences*, *63*(2), 582–597.

Schneider, U., T. Fuchs, A. Meyer-Christoffer, and B. Rudolf (2008), Global precipitation analysis products of the GPCC, *Global Precipitation Climatology Centre (GPCC), DWD, Internet Publikation*, *112*.

Sillmann, J., V. Kharin, X. Zhang, F. Zwiers, and D. Bronaugh (2013), Climate extremes indices in the CMIP5 multimodel ensemble: Part 1. Model evaluation in the present climate, *Journal of geophysical research: atmospheres*, *118*(4), 1716–1733.

Stensrud, D. J., R. L. Gall, and M. K. Nordquist (1997), Surges over the Gulf of California during the Mexican monsoon, *Monthly Weather Review*, *125*(4), 417–437.

Swain, D. L., M. Tsiang, M. Haugen, D. Singh, A. Charland, B. Rajaratnam, and N. S. Diffenbaugh (2014), The extraordinary California drought of 2013/2014: Character, context, and the role of climate change, *Bulletin of the American Meteorological Society*, *95*(9), S3.

Varuolo-Clarke, A. M., K. A. Reed, and B. Medeiros (2019), Characterizing the North American monsoon in the Community Atmosphere Model: Sensitivity to resolution and topography, *Journal of Climate*, *32*(23), 8355–8372.

Wei, X., K.-Y. Li, T. Kilpatrick, M. Wang, and S.-P. Xie (2021), Large-scale conditions for the record-setting Southern California marine heatwave of August 2018, *Geophysical Research Letters*, *48*(7), e2020GL091,803.

Wilks, D. S. (2011), *Statistical Methods in the Atmospheric Sciences*, vol. 100, Academic press.

Wills, R. C., Y. Dong, C. Proistosecu, K. C. Armour, and D. S. Battisti (2022), Systematic Climate Model Biases in the Large-Scale Patterns of Recent Sea-Surface Temperature and Sea-Level Pressure Change, *Geophysical Research Letters*, *49*(17), e2022GL100,011.

Xie, P., P. A. Arkin, and J. E. Janowiak (2007), CMAP: The CPC merged analysis of precipitation, *Measuring precipitation from space*, *28*, 319–328.

Yang, L., J. Smith, M. L. Baeck, E. Morin, and D. C. Goodrich (2017), Flash flooding in arid/semiarid regions: Dissecting the hydrometeorology and hydrology of the 19 August 2014 storm and flood hydroclimatology in Arizona, *Journal of Hydrometeorology*, *18*(12), 3103–3123.

Zhang, Q., B. Liu, S. Li, and T. Zhou (2023), Understanding Models' Global Sea Surface Temperature Bias in Mean State: From CMIP5 to CMIP6, *Geophysical Research Letters*, *50*(4), doi:10.1029/2022GL100888.